Development of nanoparticles based on amphiphilic cyclodextrins for the delivery of active substances

Luc Augis, Ingeborg Nerbø Reiten, Jan-Lukas Førde, Juan Casas-Solvas, Christina Sizun, Thomas Bizien, Ivan Rajkovic, Eric Larquet, Alexandre Michelet, Mayeul Collot, et al.

Development of nanoparticles based on amphiphilic cyclodextrins for the delivery of active substances

Luc Augis[a], Ingeborg Nerbø Reiten[b], Jan-Lukas Førde[b,c], Juan M. Casas-Solvas[d], Christina Sizun[e], Thomas Bizien[f], Ivan Rajkovic[g], Eric Larquet[h], Alexandre Michelet[i], Mayeul Collot[j], Sylviane Lesieur[a], Lars Herfindal[b], François-Xavier Legrand[*,a]

[a] Université Paris-Saclay, CNRS, Institut Galien Paris-Saclay, 91400, Orsay, France.
[b] Centre for Pharmacy, Department of Clinical Science, University of Bergen, Bergen, Norway
[c] Department of Internal Medicine, Haukeland University Hospital, 5021 Bergen, Norway
[d] Department of Chemistry and Physics, University of Almería, Ctra de Sacramento s/n, E-04120, Almería, Spain
[e] Université Paris-Saclay, CNRS, Institut de Chimie des Substances Naturelles, UPR 2301, 91198, Gif-sur-Yvette, France
[f] Université Paris-Saclay, Synchrotron Soleil, 91190, Saint-Aubin, France.
[g] SSRL, SLAC National Accelerator Lab, Menlo Park, CA, USA
[h] Laboratoire de Physique de la Matière Condensée (PMC), CNRS, Ecole Polytechnique, Institut Polytechnique de Paris, 91120 Palaiseau, France
[i] Applications Development Lab France, PerkinElmer, Villebon-sur-Yvette, France
[j] Faculté de Pharmacie, Laboratoire de Bioimagerie et Pathologies, UMR 7021 CNRS, Illkirch, France

*Corresponding author: francois-xavier.legrand[a]universite-paris-saclay.fr; +33 180 006 115

Abstract

Amphiphilic cyclodextrin derivatives (ACD) are useful starting materials for nanomedicines; however, their synthesis using enzymatic catalysis is unsatisfactory. This work focuses on a robust alternative pathway using mineral base catalysis to transesterify β-cyclodextrin with long-chain vinyl esters, yielding ACD with modular and controlled hydrocarbon chain grafting. ACDs with a wide range of degrees of substitution (DS) were reliably synthesized, as indicated by extensive physicochemical characterization, including MALDI-TOF mass spectrometry. The influence of various factors, including the type of catalyst and the length of the hydrocarbon moiety of the vinyl ester, was studied in detail. ACDs were assessed for their ability to form colloidal suspensions by nanoprecipitation, with or without PEGylated phospholipid. Small-angle X-ray scattering and cryo-electron microscopy revealed the formation of nanoparticles with distinct ultrastructures depending on the DS: an onion-like structure for low and very high DS, and reversed hexagonal organization for DS between 4.5 and 6.1. We confirmed the furtivity of the PEGylated versions of the nanoparticles through complement activation experiments and that they were well tolerated *in-vivo* on a zebrafish larvae model after intravenous injection. Furthermore, a biodistribution experiment showed that the nanoparticles left the bloodstream within 10 hours after injection and were phagocytosed by macrophages.

Keywords: amphiphilic cyclodextrin; nanoparticles; PEGylation; complement activation; zebrafish larvae

1. Introduction

Nanotechnology has brought about a revolution in the field of medicine with innovative methods for both disease diagnosis and treatment, particularly through the use of nanocarriers (Duncan and Gaspar, 2011; Khan, 2022; Kher and Kumar, 2022). Nanocarriers or nanoparticles are nanoscale structures that are designed to deliver various substances, such as drugs, genes, or imaging agents, to specific targets within the body (Couvreur and Vauthier, 2006).

The introduction of cage molecules (cyclodextrins, calixarenes, etc.) as building blocks for nanoparticle design has attracted significant attention in drug delivery purposes (Jiménez Blanco et al., 2017). The internal cavities of these supramolecules not only enable the modulation of the toxicity and bioavailability of encapsulated active substances but also contribute to enhancing their solubility. Cyclodextrins (CDs), for instance, are known for their capacity to form inclusion complexes with hydrophobic drugs, as documented in several studies (Zagami et al., 2023; Treccani et al., 2022; Challa et al., 2005; Davis and Brewster, 2004; Irie and Uekama, 1997; Komiyama, 2023; Loftsson and Brewster, 2012).

The most frequently used native CDs are cyclic oligosaccharides composed of 6, 7, or 8 glucose units, known as α-CD, β-CD and γ-CD, respectively. They are produced by enzymatic degradation of starch by glucosyltransferase. Although CDs are generally considered to be biocompatible (Davis and Brewster, 2004), their degree of toxicity varies. Cyclodextrins are typically non-toxic when used orally or topically. However, parenterally, some CDs, such as α-CD and β-CD, can exhibit cytotoxicity and nephrotoxicity due to solubilization and extraction of vital cellular components (Irie and Uekama, 1997). However, these side-effects can be significantly reduced by modifications producing derivatives such as alkyl ester-β-CD, hydroxypropyl-β-CD and sulfobutylether-β-CD; which also provide interesting new properties such as improved inclusion complexation, controlled drug delivery capabilities, and enhanced safety (Debouzy et al., 2008; Memisoglu-Bilensoy et al., 2005; Stella and He, 2008; Zhang and Ma, 2013).

CDs possess a hydrophilic outer surface and a hydrophobic inner cavity but their hydrophilic nature limits their efficacy in delivering drugs to hydrophobic environments such as lipid bilayer membranes (Wang et al., 2019). To overcome this limitation, it is possible to take advantage of the ability of amphiphilic cyclodextrins to self-organize spontaneously into nanoparticles (McNicholas et al., 2007; Quaglia et al., 2009). These amphiphilic cyclodextrin nanoparticles (ACD-NPs) possess both hydrophobic and hydrophilic properties and therefore offer several advantages over conventional CDs and other nanoparticle systems. Firstly, their expanded hydrophobic compartments allow them to encapsulate larger hydrophobic molecules and in greater amounts, resulting in improved drug loading and increased drug bioavailability (De Gaetano et al., 2023). Secondly, ACD-NPs have the capability to encapsulate hydrophilic drugs within their water-based cores (Lemos-Senna et al., 1998; Skiba et al., 1996), and within the cyclodextrin's cavity itself (Raffaini and Ganazzoli, 2007).Thirdly, the surface modification of ACD-NPs can be tailored to enhance their stability, circulation time, and targeting ability (Bandi et al., 2020; Perret et al., 2018). ACD-NPs have already been tested for the delivery of hormones, antibiotics, anti-inflammatory drugs, and antifungal agents (Skiba et al., 1995; Uekama et al., 1998).

Traditional methods for chemically modifying cyclodextrins involve intricate multi-step syntheses using protecting groups like t-butyldimethylsilyl ether, often resulting in low overall yields (Benkovics et al., 2021). Additionally, these processes present challenges due to the presence of three distinct types of alcohol on the CD, each having very specific reactivity. Several strategies have been developed to selectively modify either the primary face (Memişoğlu et al., 2002) or the secondary face (Lesieur et al., 2000), where the secondary face refers to the larger circle of the truncated cone, which is composed of 14 secondary alcohols. In contrast, the opposing primary face is composed of 7 primary alcohols. A simpler chemical approach to produce ACDs in a single step is through direct esterification or acylation of native cyclodextrins, allowing substitutions to occur freely.

Completely per-substituted cyclodextrins, whether modified on one or both sides, known as single isomers, have been observed to form NPs that exhibit noticeable differences in stability based on the nature of the substituents. CDs carrying hydrophobic chains on one side and other substituents on the other —such as halogens, PEGs, or sugars— tend to generate stable (Mendez-Ardoy et al., 2012), spontaneous (Kauscher et al., 2013; McNicholas et al., 2007; Mohan Nalluri et al., 2011; Samanta et al., 2012; Voskuhl et al., 2010), and even organized NPs (Falvey et al., 2005; Mohan Nalluri et al., 2011; Villari et al., 2013). However, CDs solely substituted with hydrophobic components, such as per-acylated β-CD with fatty acids on the secondary face and lacking any other substitutions on the primary face, tend to exhibit unstable self-arrangement (Geze et al., 2002). Therefore, when preparing NPs from CDs esterified with fatty acids, it is preferable to consider a mixture of acylated derivatives with varying numbers of chains. This mixture is commonly known as a chain-distribution derivative, contrasting with single isomeric compounds, which consist of pure molecules.

Enzymatic reactions offer a relatively straightforward method to obtain amphiphilic derivatives with a chain distribution in a single step, selectively grafting fatty acid chains onto the secondary face (Choisnard et al., 2006). However, it does have a major flaw: the median number of grafted chains, known as the degree of substitution (DS), lacks reproducibility and fluctuate between 3 and 8 (Putaux et al., 2017).

From an industrial perspective, there is a need for simple syntheses without protection and deprotection steps that can consistently produce derivatives with controlled chain distribution. In this context, we considered transesterification catalyzed by a mild mineral base, inspired by René Dicke's work on regioselective esterification of starch with vinyl acetate (Dicke, 2004).

Overall, ACD-NPs offer a promising platform for the development of nanomedicine, with potential applications in a wide range of diseases. In this work we focused on trans-esterified β-cyclodextrins using long-chain vinyl ester reagents and mineral catalysts. For the generation of ACD-based nanoparticles, we have mostly focused on C_{10} chain length derivative. This work aimed at providing a simple, robust and reproducible synthesis to facilitate the production of amphiphilic derivatives with a range of different DS. Additionally, the preparation of nanoparticles based on these modified CDs, their physical characterization and the evaluation of their toxicity were undertaken.

2. Materials and Methods

2.1 Materials

β-cyclodextrin (Kleptose ®) was kindly provided by Roquette (Lestrem, France) or purchased from CycloLab R&D (Budapest, Hungary) and dried at 50 ºC in vacuum in the presence of P_2O_5 until constant weight was reached. Vinyl decanoate (> 99.0 %), vinyl hexanoate (> 99.0 %) and vinyl 10-undecenoate (> 92.0 %) were purchased from TCI EUROPE N.V. (Zwijndrecht, Belgium). Dimethylsulfoxide (DMSO), tetrahydrofuran (THF) and inorganic catalysts: sodium hydrogen sulfate (> 90 %), sodium nitrate (> 99 %), sodium dihydrogen phosphate (> 96 %), sodium sulfate (99 %), disodium hydrogen phosphate (> 98 %), sodium carbonate (> 99.5 %), trisodium phosphate (> 96 %), lithium carbonate (99 %), potassium carbonate (99 %), rubidium carbonate (99.8 %) and cesium carbonate (99 %) were purchased from Alfa Aesar (Karlsruhe, Germany). 1,2-Dimyristoyl-rac-glycero-3-methoxypolyethylene glycol-2000 (DMG-PEG_{2000}), tetrabutylammonium fluoride solution (1 M in THF), 2,5-dihydroxybenzoic acid (2,5-DHB) (> 99.0 %), sodium chloride (NaCl) (≥ 99.0 %), *tert*-butyldimethylsilyl chloride (TBDMSCl, 97 %), imidazole (≥ 99 %), tosyl chloride (TsCl, ≥ 99 %), anhydrous copper(II) sulfate ($CuSO_4$, ≥ 99 %), sodium hydroxide (NaOH, pellets, ≥ 98 %), 30 % v/v NH_4OH (ACS) and sodium azide (NaN_3, ≥ 99 %) were purchased from Sigma-Aldrich (Saint-Quentin Fallavier, France). Methanol (≥ 99.9 %) and chloroform ($CHCl_3$) were purchased from VWR (Rosny-sous-Bois, France). Ethyl acetate (EtOAc, 99.5 %), dichloromethane (CH_2Cl_2, 99.8 %) and hexane (H, 95 %) were purchased from Panreac Applichem (Barcelona, Spain) and distilled prior to use. Dry *N,N*-dimethylformamide (DMF, AcroSeal, 99.8 %, over molecular sieves) was purchased from Acros (Geel, Belgium). Acetonitrile (CH_3CN, HPLC grade) was purchased from Scharlau (Barcelona, Spain). Thin layer chromatography (TLC) was performed on Merck silica gel 60 F_{254} aluminum sheets and developed by UV–vis light and 5 % v/v sulfuric acid in ethanol. Flash column chromatography was performed on Merck silica gel (230–400 mesh, ASTM). α-Tocopherol-BODIPY (BDP-Toco) was synthesized and provided by Mayeul Collot (Wang et al., 2021). Ultrapure water (surface tension γ = 72.2 $mN.m^{-1}$ at 22 °C; resistivity = 18.2 MΩ.cm) was produced by a Millipore Milli-Q Direct 8 water purification system.

2.2 Amphiphilic cyclodextrin synthesis

11.3 g of β-cyclodextrin (eq. to 10 g of anhydrous β-CD, i.e. 0.0088 mol) and 200 mg (2 wt.%) of inorganic catalyst (see below) were introduced in a two-neck round bottom flask and were dried at 80 °C, under stirring and reduced pressure (< 20 mbar) overnight. The temperature was then lowered to 40 °C. Anhydrous DMSO (60 mL) was added to solubilize the β-CD. In the case of reaction with vinyl decanoate (C_{10}), 31.5 mL of the latter (0.14 mol) was slowly introduced using a syringe through the septum. The heterogeneous medium was vigorously stirred (1000 rpm) and the reaction was carried out under reduced pressure for 72 hours. Concerning the two other alkyl chain derivatives made from vinyl hexanoate (C_6) and vinyl 10-undecanoate ($C_{11:1}$), β-cyclodextrin was used as reagent and sodium carbonate was used as catalyst. The reaction conditions as well as the molar ratios were the same as those described for the synthesis of the C_{10} derivative. Concerning the synthesis of azido derivatives (6^I-N_3-β-CD-C_{10} and 6^7-N_3-β-CD-C_{10}) and tert-butyldimethylsilyl (6-TBDMS-β-CD-C_{10} and 2,6-TBDMS-β-CD-C_{10}) protected derivatives, vinyl decanoate (C_{10}) was used as

reagent and sodium carbonate was used as catalyst. The reaction conditions as well as the molar ratios were the same as those described for the synthesis of the C_{10} derivative.

2.3 Purification process of amphiphilic cyclodextrins

100 mL of ultrapure water was added to the reaction medium before freezing at – 20 °C, then the mixture was freeze-dried overnight (pressure < 1 mbar; trap temperature = – 80 °C) to eliminate most of the DMSO and the vinyl reagent. The residual viscous product was homogenously dispersed by adding a sufficient volume of THF. The mixture was centrifuged at 3500 × g for 20 min, then the supernatant was recovered and the THF was removed by rotary evaporation. The solid residue obtained was ground into a fine powder before adding ultrapure water and processing to a second freeze-drying step. The final solid product, i.e., the synthesized amphiphilic cyclodextrin derivative, was dried under primary vacuum overnight.

2.4 Preparation of Heptakis(6-O-tert-butyldimethylsilyl)-β-cyclodextrin (6-TBDMS-β-CD)

6-TBDMS-β-CD was prepared according to the protocol described by (Benkovics et al., 2021).

2.5 Deprotection of 6-TBDMS-β-CD-C_{10}

The procedure described by (Ward and Ling, 2011) was followed. Briefly, 6-TBDMS-β-CD-C_{10} derivative (4.0 g, 1.98 mmol) was dissolved in THF (45 mL), and a solution of TBAF (1.0 M in THF, 40.0 mL, 40.0 mmol) was added. The reaction was stirred overnight, then the solution was concentrated under reduced pressure. The residue was dissolved in EtOAc (30 mL), and the organic solution was washed with H_2O (60 mL), saturated brine (3 × 60 mL) and dried with anhydrous Na_2SO_4. After concentration under reduced pressure, the crude compound was purified by column chromatography on silica gel as described by (Ward and Ling, 2011).

2.6 Preparation of Heptakis(2,6-di-O-tert-butyldimethylsilyl)-β-cyclodextrin (2,6-TBDMS-β-CD)

2,6-TBDMS-β-CD was prepared by a slight modification of the procedure described by (Fügedi, 1989). Briefly, β-cyclodextrin (4 g, 3.524 mmol) and imidazole (10.076 g, 148.008 mmol) were dissolved in dry DMF (100 mL) before a first amount of TBDMSCl (11.154 g, 74.004 mmol) was added in one portion. The mixture was heated at 90 °C, and the advancement of the reaction was followed by thin layer chromatography (EtOAc/Hexane 1:50) every 2-3 h until stabilized reaction yield. Then supplementary amounts of TBDSMCl (0.560 g, 3.715 mmol) and imidazole (1 g, 14.689 mmol) were added if necessary, until only one spot at R_f 0.64 was observed. Solvent was then rotary evaporated at under high vacuum at 80 ºC, and the residue was dissolved in CH_2Cl_2 (200 mL) and washed with water (2 × 100 mL). The organic phase was dried with $MgSO_4$ before solvent elimination by evaporation process. The raw product was purified by flash column chromatography (EtOAc/Hexane 1:50) to yield (2,6-TBDMS-β-CD) (8.696 g, 3.180 mmol, 90 %) as a white solid. The NMR data ($CDCl_3$) agreed with those previously described (Maynard and Vigh, 2000).

2.7 Preparation of 6^{1}-Azido-6^{1}-deoxy-β-cyclodextrin (6^{1}-N$_3$-β-CD)

6^{1}-N$_3$-β-CD was prepared in two steps. Firstly, 6^{1}-*O*-tosyl-β-cyclodextrin (6^{1}-TsO-β-CD) was synthesized by modifying the protocol described by (Law et al., 2011). Briefly, a solution of $CuSO_4$ (4.788 g, 30 mmol) in water (750 mL) and a solution of NaOH (10 g, 250 mmol) in water (750 mL) were sequentially added to a solution of β-cyclodextrin (11.350 g, 10 mmol) in water (500 mL). Subsequently, a solution of TsCl (15.061 g, 79 mmol) in acetonitrile (100 mL) was injected into the reaction solution during 1 h. The mixture was then stirred for 2 h, after which TLC (MeCN/H_2O/30 % v/v NH_4OH 10:5:2) showed the appearance of two spots identified as the monotosyl (R_f = 0.40) and ditosyl (R_f = 0.55) derivatives, in addition to starting β-cyclodextrin (R_f = 0.23). 5 % HCl was added until the mixture reached pH 7. The solid precipitate was removed by filtration and the filtrate was submitted rotary evaporation at 60 ºC until volume reduction to ~30 mL and formation of a precipitate. The resulting precipitate was recovered by filtration washed with water (50 mL) and purified by column chromatography (MeCN/H_2O/30 % v/v NH_4OH 10:3:2) to afford 6^{1}-TsO-β-CD (5.098 g, 3.955 mmol, 40 %) as a white solid. NMR data matched those previously reported in literature (B. Brady et al., 2000). In a second step, 6^{1}-TsO-β-CD (3.125 g, 2.494 mmol) and NaN_3 (0.195 g, 2.993 mmol) were dissolved in dry DMF (20 mL) and heated at 100 ºC for 2 h under N_2 atmosphere. TLC (MeCN/H_2O/30 % v/v NH_4OH 10:5:2) indicated the consumption of the starting material (R_f = 0.40) and the appearance of a spot at R_f = 0.36. The formed solid was filtered off, washed with acetone and purified by column chromatography (MeCN/H_2O/30 % v/v NH_4OH 12:3:1 → 10:4:1) to yield 6^{1}-N$_3$-β-CD (2.285 g, 1.970 mmol, 79 %) as a white solid. NMR data matched those previously reported (Bonnet et al., 2003).

2.8 Preparation of heptakis(6-azido-6-deoxy)-β-cyclodextrin (6^{7}-N$_3$-β-CD)

6^{7}-N$_3$-β-CD was prepared according to the protocol described by (Srinivasachari et al., 2008).

2.9 MALDI-TOF Mass spectrometry (MS)

2.9.1 Sample preparation

According to their solubility, samples were prepared at 1 mg.mL^{-1} in methanol/$CHCl_3$ 2:1 (v/v). 2,5-DHB was prepared at 20 mg.mL^{-1} in water/methanol 70:30 (v/v) doped with NaCl at 0.01 % (mol/mol). Two microliters of sample solution were premixed with an identical volume of matrix solution. Then, 2 µL of the mixture were deposited by the dried droplet method on a mirror polished stainless steel MALDI target and allowed to dry at room temperature and atmospheric pressure for 20 min.

2.9.2 Analysis

MALDI-TOF MS experiments were performed using an Autoflex Speed MALDITOF/TOF spectrometer (Bruker Daltonics, Bremen, Germany). This instrument was equipped with a Nd:YAG SmartBeam laser (λ = 355 nm) pulsed at a 1 kHz frequency. The mass spectrometer was operated in the reflector mode with a positive polarity. Voltages were set at 19, 16.5, 8, 21 and 9.5 kV for ion source voltage 1 and

2, lens voltage and reflector voltage 1 and 2, respectively. The extraction delay was optimized from 0 to 300 ns. Mass spectra were obtained by accumulation of 500-5000 laser shots in a *m/z* range from 600 to 5000. Laser intensity was spot-to-spot adjusted just above the ionization threshold to avoid eventual fragmentation and labile group losses, to maximize the resolution and to result in a strong analyte signal with minimal background noise. Spectra were next processed using Flex Analysis 3.3 software (Bruker Daltonics). The instrument was calibrated using standard peptide mixtures provided by the manufacturer.

2.9.3 Degree of substitution (DS)

This was determined as the median value of fatty chains grafted per cyclodextrin and was calculated from MALDI-TOF spectra using the following steps: the relative intensity of each peak was calculated according to the m/z value. Then, an increasing cumulative frequency curve was established. As shown by Figure 1, the median molecular weight was read on the abscissa axis at the intersection between 50 % intensity and the curve. Unfortunately, degrees of substitution of derivatives created from modified cyclodextrins, namely 6^1-N_3-β-CD-C_{10}, 6^7-N_3-β-CD-C_{10}, 6-TBDMS-β-CD-C_{10} and 2,6-TBDMS-β-CD-C_{10} could not be determined by mass spectrometry. We believe that these derivatives were not able to desorb from the matrix and become ionized. In this case, a combination of ^{1}H NMR spectroscopy and elemental analysis jointly made it possible to estimate the DS. DS have all been determined by MALDI-MS except when specified otherwise.

< insert Figure 1 >

2.10 ^{1}H NMR spectroscopy

Each compound (~15 mg) was dissolved in 600 µL of $CDCl_3$. All samples were measured in 5 mm NMR glass tubes. One-dimensional ^{1}H NMR spectra were recorded on a Bruker Avance III NMR spectrometer operating at a magnetic field of 16.4 T ($\nu(^1H)$ = 699.42 MHz) equipped with a PATXI probe with Z gradients, at a temperature of 25 °C. Spectra were processed with Topspin 4.0 (Bruker BioSpin) software. Baseline correction was applied to each spectrum after Fourier transformation, either with or without a 0.3 Hz exponential apodization, and phase correction.

2.11 Elemental analysis (EA)

Two measurements were made on each sample (approximately 1 mg). After calibration with various references, Elementar Vario analyzer was used for the analysis.

2.12 Liquid Chromatography-Mass Spectroscopy (LC-MS) Analysis

2.12.1 Sample preparation

The weakly substituted derivatives (DS < 4.4) were solubilized in a MeOH/$CHCl_3$ 2:1 (v/v) mixture while the others (DS > 4.4) were solubilized in pure chloroform, all at a concentration of 1 mg.mL^{-1}.

2.12.2 LC-MS measurements

Impurities in amphiphilic cyclodextrins were quantified by quaternary RSLC Dionex-U3000 liquid coupled with an LTQ-Orbitrap Velos Pro mass spectrometer (ThermoFisher Scientific, San Jose, CA). The system was controlled by XCalibur software. The separation of the compounds was carried out in normal phase liquid chromatography using a polyvinyl alcohol PVA-Sil column of dimensions 150 × 2.1 mm, 5 µm particle size purchased from YMC (Kyoto, Japan). The column oven was thermostated at 35 °C and the injector at 7 °C. Four mobile phases were used: A = heptane/ *i*PrOH 98:2, B = $CHCl_3$/*i*PrOH 65:35, C = MeOH/H_2O 95:5, D = *i*PrOH. A, B and C each contain 1 % (v/v) acetic acid and 0.08 % (v/v) triethylamine. The chromatographic table program is present in Table S1. The flow rate of the mobile phase was 400 $\mu L.min^{-1}$. A volume of 5 µL of sample was injected into the column. The ionization of the species in the mass spectrometer was done by Atmospheric-Pressure Chemical Ionization APCI (+). The APCI heater was set at 400 °C and the heated capillary at 325 °C. Sheath gas and auxiliary gas flow rates were set at 40 and 5 $L.min^{-1}$, respectively. The detection is done in full scan Fourier Transform Mass Spectrometry (FTMS, high resolution: 60,000) to be able to extract the vinyl decanoate signal via Selected Ion Monitoring (SIM) mode between 199.166 and 199.171 amu. For the determination of the fatty acid (decanoic acid), the detection was done at low resolution in transition monitoring (MRM) of the ion 173.1 $[M+H]^+ \rightarrow$ 103.0. Fragmentation was performed in CID (collision-induced dissociation) at 30 eV of collision energy in the double linear trap. For the determination of decanoic acid (DA) and vinyl decanoate (VD) amounts, a calibration was performed in the range 1.25 $ng.mL^{-1}$ to 100 $\mu g.mL^{-1}$ in pure chloroform. The limit of quantification for VD was 5 $\mu g.mL^{-1}$ and that of DA 2.5 $\mu g.mL^{-1}$.

2.13 Thermal gravimetric analysis (TGA)

TG measurements were performed with an STA 6000 thermogravimetric analyzer (PerkinElmer). Samples were placed in an open alumina crucible (200 µL) loaded in the furnace. The initial weight of the samples was around 15 mg, and nitrogen was used as the purge gas at a constant flow of 30 $mL.min^{-1}$. The weight of material was recorded during heating from 30 °C to 470 °C at a heating rate of 10 $°C.min^{-1}$.

2.14 Preparation of colloidal suspensions

2.14.1 Non-PEGylated nanoparticles

β-CD-C_{10} nanoparticles were prepared by the nanoprecipitation method. 20 mg of β-CD-C_{10} derivative was dissolved in THF (10 mL) to reach a concentration of 2 $mg.mL^{-1}$. This solution was poured drop by drop into 20 mL of distilled water (or 5 mL of 5 % w/v glucose + 15 mL of distilled water) under vigorous stirring (500 rpm). THF and most of the water were removed under reduced pressure (pressure < 10 mbar) at 45 °C until the sample volume reached 5 mL and the final concentration of β-CD-C_{10} reached 4 $mg.mL^{-1}$.

2.14.2 PEGylated nanoparticles

The preparation of the β-CD-C_{10}-PEG_{2000} NPs followed the same procedure as that for non-PEGylated nanoparticles, except that a defined amount of DMG-PEG_{2000} was

dissolved in THF at the same time as the β-CD-C_{10} derivative. For derivatives with a DS greater than 5, 33 mol% of DMG-PEG_{2000} was introduced. However, only 8 mol% and 16 mol% of DMG-PEG_{2000} were introduced for DS of 3.7 and 4.5, respectively.

2.14.3 Fluorescent nanoparticles

0.5 mol% of BDP-Toco was dissolved in THF with the ACD derivative with or without DMG-PEG_{2000}.

2.15 Nanoparticle size and zeta potential measurements

The particle size was determined by Dynamic Light Scattering (DLS) using a Zeta Sizer ZS90 (Malvern Instruments). Measurements were made in intensity mode, at 25 °C with a fixed angle of 90° and 633 nm laser beam. Nanoparticles at originally 4 $mg.mL^{-1}$ were diluted 8 fold using either Milli-Q water or glucose 5 % (w/v). The zeta potential was parallelly determined by using the same apparatus Zeta Sizer ZS90 (Malvern Instruments). NPs at originally 4 $mg.mL^{-1}$ were diluted by a factor 4 using glucose 5 %. Zeta potential values were obtained from electrophoretic mobility using the Hückel equation.

2.16 Small-Angle X-ray Scattering of non-PEGylated NPs in MilliQ water

SAXS experiments were performed at the BioSAXS beamline 4-2 of the Stanford Synchrotron Radiation Lightsource (SSRL) using a slit-collimated monochromatic X-ray beam. The samples were loaded into a quartz capillary by an automated sample changer system (Martel et al., 2012) and each sample was exposed to X-rays 10 times for 1 second to record 2D SAXS patterns. The sample capillary was thoroughly washed after each sample to prevent cross contamination. SAXS experiments were done with 11 keV energy X-rays and a sample to detector distance of 1.1 m resulting in a 0.013 - 0.7 $Å^{-1}$ vector range. The data were acquired using a Dectris Pilatus3 X 1M. 2D scattering data were azimuthally integrated using the SasTool program which calculated averaged one-dimensional intensity (I(q)) versus scattering vector (q) profiles. To account for background, intensity from the dispersion medium alone was subtracted from the scattering intensity recorded from each sample solution.

2.17 Small-Angle X-ray Scattering of non-PEGylated NPs in glucose 5 %; PEGylated NPs in MilliQ water and glucose 5 %.

SAXS measurements were performed on the high brilliance SWING beamline at the Soleil synchrotron facility, with monochromator set at 12 keV (David and Pérez, 2009). Using a EIGERX 4M detector, diffraction patterns were recorded for reciprocal spacing varying between 6.06×10^{-4} $Å^{-1}$ and 0.7569 $Å^{-1}$; that is, repetitive distances ranging from 8.3 Å to 10,368 Å. 1D SAXS curves were obtained by circular averaging of the 2D images using the Foxtrot software. As no difference was observed between the 5 images recorded for each sample, the 1D curves were averaged to obtain 1 curve for each sample and references with better statistics (to improve noise to signal ratio).

2.18 Cryo-electron microscopy (Cryo-EM)

Four µL of nanoparticle suspensions were deposited on a 300-mesh lacey carbon-coated grid. After blotting with filter paper, the grid was frozen by rapid plunging in liquid ethane and was mounted and inserted in the microscope using a nitrogen-cooled side entry Gatan Elsa™ (698) cryo-holder at a temperature of − 181 °C. Observations were carried out in a ThermoFisher Scientific G3 Titan Themis 300 transmission electron microscope equipped with a cryo-box anticontamination system and a C-Twin objective lens (Cs = 2.7 mm, Cc = 2.7 mm, Focal length = 3.5 mm), using an accelerating voltage of 300 kV, with the following illumination conditions: spot size of 5, a 150 µm condenser aperture, and no objective aperture. Images were recorded (defocus range: − 0.3 to − 0.4 µm), using the low electron dose system (10 $e^{-}/Å^{2}$ per sec), with a magnification of 28,500 ×, 58,000 × and 98,000 × on a ThermoFischer Scientific™ Falcon 3EC Direct Detection Electron 4K × 4K camera in linear mode (exposition time: 1 sec).

2.19 Activation of the complement system

Activation of the complement system induced by the nanoparticles was evaluated using a 2D immunoelectrophoresis technique, outlined in detail in references (Bertholon et al., 2006; Boackle et al., 1983). The volume of the nanoparticles as well as the volume of the dilution solvent were calculated to have the same surface area of 485 $cm^{2}.mL^{-1}$ for every batch of nanoparticles. The concentration and the hydrodynamic radius of the nanoparticles were taken into consideration for this. Once the nanoparticles were diluted, 12.5 µL of veronal buffered saline (VBS) and 12.5 µL of human serum were added one after the other. Each sample was incubated for 1 hour at 37 °C. After incubation, 3 µL of each sample were subjected to a first electrophoresis on a 1 % agarose gel. The second-dimension electrophoresis was carried out on Gelbond® films in 1 % agarose gel plates containing a polyclonal human Complement C3 antibody (Anti-Complement C3 antiserum produced in goat, Sigma-Aldrich, France), recognizing both C3 and C3b. The films were finally dried and stained with Coomassie blue to reveal the presence of C3 and C3b, which both react with the antibody. The complement activation factor was calculated from the ratio of the area of the peak attributed to C3b over the sum of the areas of the peaks attributed to C3b and to C3. VBS composition was modulated by divalent cations, to reproduce different activation pathway. Two types VBS solutions were used in this study: VBS^{2+} and VBS-EGTA-Mg^{2+}. VBS^{2+} containing 5 mM diethylmalonylurea, 0.15 mM calcium chloride, 0.5 mM magnesium chloride, 150 mM sodium chloride, pH 7.4 was used to investigate complement activation triggered by all pathways. VBS-EGTA-Mg^{2+} containing 5 mM diethylmalonylurea, 0.1 M magnesium chloride, 150 mM sodium chloride, 10 mM EGTA pH 7.4 was used to investigate complement activation triggered by calcium-independent pathways. It is noteworthy that the composition VBS^{2+} and of VBS-EGTA-Mg^{2} corresponded to those generally found in the literature and in commercial assays to assess *in-vitro* evaluation of complement activation (Des Prez et al., 1975).

2.20 In-vivo experiments (toxicity and biodistribution)

2.20.1 Zebrafish husbandry

Zebrafish (Danio rerio) of the transparent strain Casper were housed under standard conditions at the zebrafish facility of the University of Bergen. Fertilized zebrafish eggs were incubated at 28.5 °C in E3 medium (“Cold Spring Harb Protoc,” 2011) All

zebrafish embryos were euthanized prior to reaching 5 DPF. Euthanasia was performed by cooling dishes containing embryos on ice for 20 minutes followed by freezing overnight. Transgenic zebrafish larvae of the *Casper* strain with fluorescent macrophages expressing tol2-mpeg:mCherry were used to study the macrophage uptake of NPs. The Tol2-mpeg1-mcherry plasmid (Addgene plasmid #58935) was from Anna Huttenlocher ("Addgene," n.d.).

2.20.2 Zebrafish injections

During injections and imaging, zebrafish embryos were sedated using E3 medium containing 0.16 $mg.mL^{-1}$ tricaine methanesulfonate (Sigma Aldrich). Sedated embryos at the long-pec stage (Kimmel et al., 1995) were placed on a bed of 2 % agarose (Sigma-Aldrich) and injected into the posterior cardinal vein using microinjection pipettes with 4 µm inner diameter (VICbl-4-0-0-55, BioMedical Instruments, Germany) fitted on a Narishige MMN-5 and MMO-220A micromanipulator system connected to a FemtoJet 4x (Eppendorf). For each sample, the injection time was kept constant at 0.1 second and injection pressure was adjusted to produce a droplet with diameter of 200 µm in peanut oil, measured with a 1mm ruler (Thorlabs, NJ).

2.20.3 Zebrafish imaging

The zebrafish were imaged using a Andor Dragonfly 505 confocal spinning disc system with an inverted Nikon Ti-E microscope and an iXon 888 Life EMCCD. Both brightfield, red and green fluorescence was acquired during the same scan. For red fluorescent imaging, a 561 nm excitation laser and 600/25 nm bandpass filter were used. For green fluorescent imaging, a 481 nm excitation laser and 525/25 nm bandpass filter were used. The acquired images were processed using the ImageJ distribution Fiji (Schindelin et al., 2012). For illustration, the fluorescent stack was processed using a max projection.

2.20.4 Zebrafish heartrate monitoring

For heartrate monitoring, zebrafish embryos were filmed for approximately 10 seconds using a M205 FA (Leica). The heartrate was then measured using the Fiji macro described in (Førde et al., 2022)

2.20.5 Statistical analysis

Mixed-effects analysis (MEA) was preferred over the two-way ANOVA test as it is more flexible, can handle unbalanced data with missing values due to deaths, and accounts for random effects, such as variation between batches of larvae.

3. Results and discussion

3.1 Synthesis of the amphiphilic cyclodextrin derivatives

Acylation of β-cyclodextrin was performed via transesterification of its alcohol groups using different vinyl esters as reagents and a mild mineral base as catalyst (Figure 2.A). Due to its ability to deprotonate alcohols, sodium hydroxide could have been a convenient catalyst. However, it produces water as a byproduct, which can lead to hydrolysis of the esters formed. Consequently, this base was excluded from consideration. Vinyl decanoate (C_{10} chain length) was chosen for most of our syntheses, leading to β-CD-C_{10} derivatives which exhibit a higher compression elastic modulus than β-CD-C_n (n = 8, 12 or 14) at DS > 5 (Putaux et al., 2017). Vinyl esters are convenient for these syntheses as they produce acetaldehyde gas as a by-product. Immediately after its formation, this gas was extracted from the reaction medium through the pump, effectively inhibiting the reverse reaction and thereby facilitating the achievement of high yields. As there are 21 alcohols available per cyclodextrin, the resulting compound is a statistical mixture. The degree of substitution (DS), which indicates the median number of attached fatty chains, was determined through MALDI-TOF mass spectrometry (Figure 1). The impact of various factors, such as heating temperature, catalyst pKa, and cationic counter ion radius, on the DS was investigated.

First, a range of sodium-based catalysts was employed to highlight the impact of the catalyst pKa on the DS. Our results (Figure 2.B) showed that the obtained DSs displayed a strong correlation with aqueous pKas from (Parsons, 1967), even though our synthesis took place in DMSO, a polar and aprotic solvent differing from aqueous conditions. From our understanding, it is clear that stronger bases lead to the deprotonation of more alcohols, resulting in the production of higher substituted β-CD derivatives. In a second step, the effect of the cationic counter ion was investigated using carbonate-based catalysts. The use of larger cations (K^+, Rb^+, and Cs^+) yielded higher DS derivatives in contrast to the use of smaller cations (Li^+ and Na^+), as shown in Figure 2.C. Our hypothesis is that larger cations would result in weaker [CD-O^- – $cation^+$] bonds due to the asymmetric electron density. This would make oxygen electrons more available to attack the carbonyl of the vinyl ester reagent. The influence of both, the heating temperature, and the quantity of catalyst on the DS were also investigated (Figure S1), however, their influences were not as sharp as the effect of the catalyst's nature. We conclude that the catalyst selection alone is the key-variable for obtaining a derivative with the desired DS. Overall, we generated a total of 22 batches of β-CD-C_{10} derivatives through varying synthesis conditions. The synthesis consistently produced satisfactory yields (Table S2) for derivatives with a DS below 13, averaging around 79 ± 8 %. However, beyond a DS of 13, the yields declined to approximately 55 ± 5 %, primarily attributed to both the inherent steric hindrance of the chains and the challenges associated with purifying highly hydrophobic derivatives. The reaction mechanism can be found in the supporting information (Figure S2).

We assessed the reproducibility of the synthesis under the following conditions: using vinyl decanoate as the reagent, sodium carbonate as the catalyst, at 40 °C for 72 hours. Sodium carbonate was selected as the catalyst due to its ability to generates derivatives with mid-range DS, typically hovering around 8. To save resources, we conducted three smaller-scale syntheses using 1 g of anhydrous β-CD instead of the usual 10 g. The synthesis based on 10 g yielded a derivative with a median DS of 8.1,

while the three smaller syntheses produced DS values of 8.0, 8.6, and 8.6, as calculated from their mass spectra (Figure S3). The β-CD acylation using this reaction procedure demonstrated good reproducibility.

< insert Figure 2 >

In order to investigate the influence of the alkyl chain length, two syntheses were carried out using vinyl esters with different alkyl chain lengths: vinyl hexanoate (C_6) and vinyl 10-undecenoate ($C_{11:1}$), at a reaction temperature of 40 °C using sodium carbonate as a catalyst. These syntheses resulted in derivatives with DS values of 11.7 and 7.2, respectively (Tables S3 and S4). This demonstrates the possibility of using reagents with various chain lengths, with or without unsaturation. Under the same reaction conditions, a synthesis using vinyl decanoate (C_{10}) produced a compound mixture with a DS of 8.1. Therefore, the chain length appears to have an impact on reactivity, the longer the vinyl ester chains are, the more they will obstruct possible future substitutions, leading to a lower DS.

In order to understand the positioning of the grafted chains, particularly their presence on the primary or secondary face depending on the DS, we investigated the reactivity of β-cyclodextrin's hydroxyl groups. We examined the reactivity of the C3 hydroxyls by using partially protected cyclodextrins with *tert*-butyldimethylsilyl reagent at positions C2 and C6 (referred to as 2,6-TBDMS-β-CD). This CD was used as starting material in standard synthesis conditions with vinyl decanoate as the reagent and sodium carbonate as the catalyst. The results presented in Tables S5 and S6 indicate that the 2,6-TBDMS-β-CD-C_{10} derivative has a degree of substitution of 0.8 from NMR and 2.1 from EA, demonstrating the very low reactivity of the C3 hydroxyls. Next, to assess the reactivity of the C2 hydroxyls, we employed two cyclodextrins modified on the primary face: heptakis(6-*O*-*tert*-butyldimethylsilyl)-β-cyclodextrin and heptakis(6-azido-deoxy)-β-cyclodextrin, referred to as 6-TBDMS-β-CD and 6^7-N_3-β-CD, respectively. These cyclodextrins were used as starting materials under normal synthesis conditions, with vinyl decanoate as the reagent and sodium carbonate as the catalyst. The DS for the 6-TBDMS-β-CD-C_{10} derivative was found to be 3.0 from NMR and 4.5 from EA, while the 6^7-N_3-β-CD-C_{10} derivative exhibited a DS of 8.5 from NMR and 7.4 from EA (Tables S5, S7 and S8). The derivative produced from native β-CD under the same conditions had a DS of 8.1. Comparing these results with the β-CD-C_{10} derivative, the two protected derivatives offered distinct conclusions. Either 100 % of the first grafts happens on the secondary face (β-CD-C_{10} vs. 6^7-N_3-β-CD-C_{10}) or the reactivity of C2 and C6 is equivalent (β-CD-C_{10} vs. 6-TBDMS-β-CD-C_{10}).

These results align with the anticipated reactivity of native β-cyclodextrin. First, considering their reactivity in aqueous medium, the hydroxyl groups in C2 position (at the secondary face) are the most acidic (pKa = 12 – 13) and due to an intramolecular H-bonding network, the C3 hydroxyls are the least reactive (Benito and García Fernández, 2019; Gaidamauskas et al., 2009; Rong and D'Souza, 1990). The pKa of the C6 alcohol can be compared to other primary alcohols, around 15 – 16 (Benito and García Fernández, 2019; Rong and D'Souza, 1990). The esterification of β-CD is highly dependent on the deprotonation of its alcohols, with the C2 position being the first to be deprotonated, followed by C6, and finally C3. Despite steric hindrance being suspected to play a role during the substitution process, it is conceivable that the seven

first substitutions predominantly occur on the secondary face (C2 and C3 hydroxyls) of the β-cyclodextrin. Beyond this, as the DS exceeds 7, partial substitution of both the primary (C6 hydroxyls) and secondary faces become more likely.

Secondly, it is crucial to consider the physico-chemical properties of the anhydrous dimethyl sulfoxide (DMSO) solvent used. DMSO is highly polar, allowing for the dissolution of mineral catalysts through dipole-dipole interactions, as well as the solubilization of our reagents (β-CD and vinyl esters) through van der Waals bonds. Assessing the reactivity of β-CD hydroxyls in DMSO is very challenging since the available pKa values in the literature only relate to simple alcohols such as methanol, ethanol, and isopropanol (Olmstead et al., 1980). Considering ethanol (EtOH), a primary alcohol, and isopropyl alcohol (*i*PrOH), a secondary alcohol, as equivalents to the alcohols in positions C6 and C2 of the β-CD, their experimental pKa values in DMSO are very similar; 29.8 for EtOH and 30.2 for *i*PrOH, indicating no significant priority between them. An interesting study using an empirical method to convert pKa values between different solvents could have been insightful (Rossini et al., 2018). Unfortunately, they did not succeed in establishing a proper shift value for the alcohol family.

3.2 Extension to derivatives of chemical interest: mono- and per-azido derivatives

We conducted experiments to evaluate our synthesis approach on cyclodextrins of chemical significance, using the standard reaction conditions. The starting materials were β-cyclodextrins substituted with azido groups (N_3) either on a single hydroxyl at C6 position, referred to as 6^1-azido-6^1-deoxy-β-cyclodextrin (6^1-N_3-β-CD), or on all C6 hydroxyls, referred to as heptakis(6-azido-deoxy)-β-cyclodextrin (6^7-N_3-β-CD). The azido groups present on amphiphilic cyclodextrins can readily react with alkyne compounds, providing a diverse range of interesting cyclodextrins through the well-known click reaction. Our results indicate that the grafting of C_{10} chains from vinyl decanoate led to a 6^1-N_3-β-CD-C_{10} derivative exhibiting a 15.0 DS from NMR and 12.7 DS from EA, and to a 6^7-N_3-β-CD-C_{10} derivative with a 8.5 DS from NMR and 7.4 DS from EA as illustrated in Tables S5, S8 and S9. Hence, our synthesis approach is suitable for this category of modified cyclodextrins.

3.3 Quantification of impurities and volatiles

Vinyl decanoate (VD) possesses amphiphilic properties, meaning that any remaining molecules could potentially be incorporated into future NPs during the nanoprecipitation process. The same reasoning applies to decanoic acid (DA), which is a by-product that may result from the hydrolysis of esters. This reaction could take place in the presence of moisture. Additionally, any trace of remaining solvents may increase *in-vivo* toxicity. So, before proceeding to the next stages, it was essential to evaluate the purity of our derivatives. First, thermogravimetric analysis was performed on all derivatives produced i.e., 22 batches. This technique estimated the total content of volatile species, with boiling points below 275 °C, including THF (66 °C), water (100 °C), vinyl decanoate (119 °C), DMSO (189 °C), and decanoic acid (269 °C). We found a range of 1.36 wt.% to 5.46 wt.% of impurities, as shown in Table S2. Unfortunately, no correlation was observed between the degradation temperature (T_{ONSET}) and the degree of substitution (Figure S4), thus TGA could not be used for DS estimation. To go further, the amount of residual DMSO and water was determined by ^{1}H NMR,

revealing a range from 0.00 wt.% to 1.02 wt.% and 0.00 wt.% to 0.08 wt.%, respectively. LCMS was used to quantify the amounts of vinyl decanoate and decanoic acid. These were found to be below the detection for VD (0.5 wt.%) and up to 1.10 wt.% for DA. The purity value finally considered was the one determined through thermogravimetric analysis. For a comprehensive overview, Tables S10–S31 contain measurements for all 22 β-CD-C_{10} samples, including the ^{1}H NMR and MALDI-MS spectra, TGA thermograms, and SAXS patterns.

3.4 Morphology and ultrastructure of self-assembled nanoparticles

We prepared colloidal suspensions using the nanoprecipitation process for a total of 22 batches of β-CD-C_{10} derivatives, along with β-CD-C_6 and β-CD-$C_{11:1}$ derivatives. To determine the average hydrodynamic diameter, we employed Dynamic Light Scattering. The size of β-CD-C_{10} NPs ranged from 146 to 277 nm, depending on the DS. Interestingly, we observed that amphiphilic CDs with a lower DS tended to result in larger nanoparticles, as detailed in Table S32. Furthermore, when comparing the NPs from β-CD-C_6 and β-CD-$C_{11:1}$ derivatives, we found that they had sizes of 203 nm and 102 nm, respectively. Notably, the smallest nanoparticles were obtained from the derivative with the longest chains.

Following nanoprecipitation, SAXS measurements were conducted on all the NPs derivative to determine whether they exhibited an ultrastructure. As indicated in Table S32, certain nanoparticles displayed a distinct internal structure, such as a lamellar or inverse hexagonal arrangement, with multiple-order peaks, while others showed only a single diffraction peak. Consequently, for cryo-EM imaging, *in-vitro* and *in-vivo* experiments, we chose to focus on a subset of 7 derivatives that initially displayed interesting self-organization. Also, we specifically chose these derivatives to cover the full spectrum of DS, ranging from 3.7 to 14.7, with increment steps of approximately 2. Morphological characteristics of the selected NPs are presented in Table 1.

< insert Table 1 >

Through SAXS measurements and cryogenic transmission electron microscopy (cryo-EM) imaging (Figures 3 and 4), it was found that the low DS derivative (DS = 3.7) forms an onion-like structure with an inter-lamellar distance of 39.5 Å. Derivatives with a DS between 4.5 and 6.1 clearly self-organize according to an inversed hexagonal structure. The SAXS profiles of derivatives with DS between 8.1 and 10.5 do not exhibit clear evidence of either hexagonal or lamellar packing, as shown by the absence of second-order peaks. However, the angular sides of the particles observed in cryo-EM are consistent with a hexagonal-like supramolecular organization. The SAXS experiment conducted on the DS 12.4 derivative showed a single peak reflection without sufficient repeat units to identify the NP internal structure. However, cryo-EM investigation supported a lamellar-like organization. Thus, derivatives with DS between 12.4 and 14.6 self-organize into a lamellar phase, with interlamellar distances of about 28 Å. These distances are much shorter than those calculated on DS 3.7. Unlike DS 3.7, the cyclodextrins in this case possess alkyl chains on both sides, causing the chains to face each other and allowing for potential intercalation between them. This phenomenon has been previously observed and accounts for the reduction in inter-lamellar distance (Putaux et al., 2017).

Additionally, in preparation for the upcoming biological experiments, we also produced NPs in a 5 % glucose medium. In these conditions, DS 10.5 NPs exhibited diffraction peaks corresponding to order 2 ($\sqrt{3}q_1$) and order 3 ($2q_1$) related to inverse hexagonal packing (diffraction profiles are presented in Figure S5 and the interpretation in Table S33). This information suggests that the range of DS (8.1 to 10.5) exhibits poor organization and may represent NPs in a transitional state ($L_\alpha \rightarrow H_{II}$).

< insert Figure 3 >

< insert Figure 4 >

The critical packing parameter (CPP) is a commonly used measurement to explain how amphiphilic molecules tend to arrange themselves into specific structures. It takes into consideration the overall shape of a molecule, including the size of the polar head and the characteristics of the hydrophobic tail. The CPP is calculated using this formula:

$$CPP = \frac{v}{a_0 \times l_c} \quad (1)$$

Where v is the volume of the hydrophobic chains, a_0 is the effective head group area at the hydrophobic-hydrophilic interface and l_c is the length of the hydrophobic chains. When CPP value falls between 0.5 and 1, the molecule's shape resembles an inverted truncated cone, which facilitates the formation of flexible bilayers and micelles. When CPP ≈ 1, the molecule has a cylindrical shape, promoting the formation of lamellar organizations. On the other hand, when the CPP exceeds 1, the molecule adopts a conical shape and tends to organize itself into inverse hexagonal structures. The CPP approach is a useful tool for analyzing amphiphilic molecules that have a polar head and a single nonpolar tail (Khalil and Zarari, 2014). Our derivatives satisfy these criteria, but only when the degree of substitution is below a certain threshold, estimated to be around 5. Beyond this limit, additional chains can be attached to the primary face, resulting in two distinct hydrophobic compartments. Despite this limitation, we have estimated the overall molecular shapes and the CPP values based on the DS (Figure 5), taking into consideration the reactivity of the alcohols, steric constraints, and the observed ultrastructures.

The 6-TBDMS-β-CD-C_{10} derivative, after deprotection, was found to have a DS of 1.7 according to mass spectrometry (Table S34). Interestingly, it exhibited characteristics different from those of the other derivatives. It was soluble in water and did not display the Tyndall effect typically observed when large molecular aggregates form (Lin and Haynes, 2010). Additionally, it showed foaming behavior when shaken, leading to the conclusion that micelles are formed when it is solubilized. After exceeding an unknown DS limit, between 1.7 and 3.7, any extra chains added would still attach to the secondary face. However, in this case, they would contribute to a more cylindrical shape, promoting the formation of a lamellar packing (L_α). As more chains are added, the density of the secondary face increases, leading to steric hindrance and eventual grafting onto the primary face. When the secondary face is partially substituted with only a few chains present on the primary one, the overall molecular shape tends towards a conical shape. This shape promotes the formation of negatively curved

assemblies and the emergence of an inverse hexagonal ultrastructure (H_{II}). For DS ≥ 8.1, although the secondary face becomes almost fully substituted, the substitution pattern continues on both sides. This causes the overall molecular shape to transition from a mixture of both shapes to a second fully substituted cylindrical shape at DS ≥ 12.4.

The phase change limit at DS ≈ 5 has been previously observed in the study conducted by (Putaux et al., 2017). They worked on acylated β-cyclodextrin by enzymatic transesterification and found that before reaching DS ≈ 5, lamellar organizations were observed, while inverse hexagonal ultrastructures were observed above this threshold. Their synthesis procedure mostly substitutes on the secondary face, which limited their range of DS from 3 to 7. Although our production method differs from theirs, our results corroborate their findings and provide additional insights over a broader range of DS values.

< insert Figure 5 >

3.5 Stability of self-assembled nanoparticles

The stability of the 22 NPs batches was estimated by monitoring their average hydrodynamic average diameter and the polydispersity index (PdI) by Dynamic Light Scattering (DLS). Measurements were done immediately after preparation and at intervals of about 50, 100, 175, and 330 days for the nanoparticles prepared in water (Figure S6). The influence of storage temperature on the stability was also investigated. Once nanoprecipitated, each dispersion was divided into two equal parts and stored in a refrigerator (4 °C) or in a temperature-controlled room (18 °C). In both cases, the nanoparticle size changed by less than 5 %, and the PdI value remained below 0.05, indicating a highly monodisperse population (“Malvern,” 2017). Regardless of the storage temperature, the nanoparticles prepared in pure water were highly stable over the study period, which lasted almost a year. However, the stability of these neutral and uncharged amphiphilic cyclodextrin nanoparticles is affected by various factors when exposed to a saline medium, including the ionic strength, solvation properties, and the screening effect. As a result, the ACD-NPs tended to aggregate rapidly in saline solutions such as phosphate-buffered saline. It is important to note that this aggregation phenomenon is not unique to our NPs, as it has also been observed in other studies (Yaméogo et al., 2014).

3.6 Morphology, ultrastructure and stability of PEGylated nanoparticles

The incorporation of PEG into the nanoparticles is a well-known method for enhancing their stability and improving their persistence within the vascular system (Yaméogo et al., 2014). In pursuit of this objective, we prepared fresh PEGylated NPs analogues to those seven previously selected (Table 1) by dissolving DMG-PEG_{2000}, acting as the stealth agent, alongside the corresponding β-CD-C_{10} derivative in THF. Subsequently, nanoprecipitation was carried out either in purified water or in a 5 % glucose solution. As shown in Figure 4, the introduction of PEG not only preserved the original ultrastructure of the NPs but also significantly improved it. Particularly noteworthy is the observation that NPs with DS 8.1 and 10.5 displayed a clear inverse hexagonal organization in the cryo-EM images, in contrast with the non-PEGylated analogue NPs. This was confirmed by the fast Fourier transform analysis, revealing distinct six-fold

symmetry. Additionally, we confirmed the preservation of the internal structure of the PEGylated NPs in both aqueous and glucose media through small-angle X-ray diffraction (Figure S5). Furthermore, a 5 % increase in the d_{100} distance was observed (Table S33), which results from the introduction of PEG into the aqueous compartments of the NPs. The size of a few PEGylated derivatives prepared in distilled water (Table 2) was also monitored over time, and although their polydispersity was larger, they also remained stable for almost a year as shown in Figure S6.C.

< insert Table 2 >

3.7 Toxicity

The toxicity of seven PEGylated nanoparticles (PEG-NPs) was assessed using a zebrafish larvae model. Four µL of the PEG-NP solutions were injected into 12-13 zebrafish larvae at two days post-fertilization (DPF). During the observation period, 2 out of 12 zebrafish larvae injected with DS 3.7 and 6.1 died after 24 hours (Figure 6.A). However, we also observed one death in the group receiving 5 % glucose solution and no malformations or toxic effects were observed during the study period, leading to the conclusion that the observed deaths were probably caused by manual handling or transportation during anesthesia and not by the presence of the PEG-NPs in the blood.

Heart rates were monitored at 24, 48, and 72 hours after injection (HPI) of PEG-NPs. We did not observe any change in heartrate of the injected larvae compared to controls at 24 and 48 HPI. Through mixed effect analyses (MEA) we found that the heartrate of zebrafish larvae injected with any PEG-NPs decreased after 72 hours compared with Glu 5 % group (Figure 6.B). The effects on the heartrate could be caused by PEG-NP degradation products such as fatty chains and DMG-PEG molecules. To study this, we injected either PEGylated or non-PEGylated DS 8.1 nanoparticles, as well as DMG-PEG_{2000} on its own. The DMG-PEG_{2000} solution was prepared by dissolving the same quantity as that present in the DS 8.1 group i.e., 1.4 $mg.mL^{-1}$, in 5 % glucose. In this test we found no change in heartrate at any time point, as illustrated in Figure 6.C. An additional toxicity test was conducted with non-PEGylated NPs (Figure S7), which demonstrated a 100 % survival rate across all DS (N = 10 each). From these tests we conclude that the NPs have no or very low toxicity towards zebrafish larvae, and thus good potential as a drug-carrier with high biocompatibility.

< insert Figure 6 >

3.8 Fluorescent labelling

The BODIPY (BDP) fluorescence molecule was chosen to allow the colocalization of nanoparticles (in green) and zebrafish macrophages (in red). Instead of chemically attaching BDP to the β-CD-C_{10} derivatives, we used a new probe synthesized from α-tocopherol and BDP (Wang et al., 2021). The alkyl chain (C_{13}) of α-tocopherol can form a stable complex by being included in the internal cavity of β-CD (Aytac and Uyar, 2016). The acylation of β-CD probably enhanced the complexation of α-tocopherol, as it enabled its inclusion not only inside the internal cavity but also within the fatty chains. Thus, in order to prepare PEG-NPs labelled with BDP, BDP-Toco was dissolved in THF along with the corresponding β-CD-C_{10} derivative and DMG-PEG_{2000}. The hydrodynamic diameters of the labeled PEGylated NPs in glucose 5 %, measured by

DLS, showed a slight variation, on average 4 %, compared to the non-labeled PEGylated NPs (Table S35). The stability of the PEGylated fluorescent NPs was not studied. However, when we conducted biodistribution experiments within 5 days of preparation, we did not observe any visible signs of aggregation.

3.9 Immune response and biodistribution

The complement system is a part of the immune system that plays a crucial role in recognizing and eliminating foreign particles, including NPs. Activation of the complement system can lead to various immune responses, including inflammation and potential adverse effects. The ability of several types of PEGylated and non-PEGylated β-CD-C_{10} nanoparticles to activate the complement system was measured by analyzing the cleavage of complement C3 protein in serum through 2D immunoelectrophoresis. All NPs used in these experiments were nanoprecipitated in glucose 5 %; consequently this medium was considered as our non-activating reference. However, although a 5 % glucose solution is not expected to activate the complement system, we detected between 25 to 30 % activation (Figure 6.D). To verify the reliability of the experiment as well as the quality of the human serum, a negative control was performed. VBS^{2+} was replaced by VBS EDTA, without any dilution in glucose 5 %. In these conditions, no divalent cation is available in the samples. These ions are needed for the functioning of the complement cascade. Therefore, without divalent cation, the complement cascade cannot be activated. The complement activation factor (CAF) observed with VBS-EDTA was 7 ± 1 %, suggesting that the quality of the serum being tested was acceptable.

Non-PEGylated NPs exhibited an average activation level 17 % higher than the glucose reference solution when tested in VBS^{2+} buffer, with the exception of 4.5 DS NPs. However, when tested in VBS-EGTA-Mg^{2+} buffer, the same NPs showed a further increase in activation of approximately 19 % compared to the glucose reference. The use of this buffer highlights the triggered activation pathway. VBS-EGTA-Mg^{2+} does not contain calcium ions, which are necessary for the classical and lectin pathways unlike the alternative pathway. The activation values of our NPs were similar in both buffers, indicating that activation is not calcium-dependent and occurs through the alternative pathway. Complement activation is typically influenced by the surface charge of the nanoparticles, as it has been previously reported that a high surface charge, whether positive or negative, can initiate interactions with complement proteins, particularly through the alternative pathway (Morille et al., 2010; Yaméogo et al., 2014). Therefore, we measured the zeta potential of the NPs by DLS, obtaining values ranging from – 28.1 to – 9.1 mV for non-PEGylated NPs (Table 1). Neither the degree of substitution nor the internal organization of the NPs seemed to have a clear impact on the results. For unknown reasons, the 4.5 DS NPs activated the most although their surface charge is moderate compared to NPs with other compositions.

In the case of PEGylated NPs, the surface potential was more moderate, ranging from – 11.0 to – 5.0 mV, as shown by Table 2. As expected, due to steric repulsions, the PEGylated NPs triggered about 30 % less activation than the non-PEGylated NPs. In order to observe the biodistribution of the PEG-NPs and their interaction with macrophages, we injected PEG-NPs labeled with green fluorescence intravenously into 2-DPF zebrafish larvae expressing the red fluorescent macrophages. The larvae were imaged at 3, 24, and 48 HPI, as illustrated in Figure 7. Several studies have

demonstrated that nanoparticle toxicity and biodistribution are directly linked to size (Chithrani et al., 2006; Sriram et al., 2012) and shape (Chithrani et al., 2006; Huang et al., 2011; Stoehr et al., 2011). Therefore, we wanted to compare the dispersions of labeled PEG-NPs with DS 3.7, 6.1, and 14.6 to highlight possible differences between size and shape, where DS 3.7 and DS 14.6 were both spherically shaped with respective sizes of 131 ± 2 nm and 218 ± 4 nm, while DS 6.1 and 14.6 had similar size but elongated and spherical shapes respectively. Table S35 gives details of NP size as a function of the medium, PEGylation and the incorporation of the fluorescent marker.

< insert Figure 7 >

At 3 HPI, all PEG-NPs were still circulating in the blood stream and were particularly visible in the large blood vessels, such as the posterior cardinal vein and dorsal aorta (Figure 7, white arrows). At 24 HPI, there was less fluorescence observed in circulation for all PEG-NPs, and several larger yellow objects appeared in the tail region, indicating uptake of the green PEG-NPs by the red macrophages. For DS 14.6, there also appeared to be aggregates of the nanoparticles appearing as smaller green objects which had not been engulfed by macrophages and were still circulating at 48 HPI. Such objects were also observed for DS 3.7, but to a much lesser extent than for DS 14.6. For DS 6.1, almost no green fluorescence was observed outside of macrophages at 48 HPI. DS 6.1 PEG-NPs had the same hydrodynamic diameter as DS 14.6, which could indicate that elongated nanoparticles are eliminated more quickly than spherical ones. To more precisely estimate the time at which the nanoparticles escaped the bloodstream, short timelapse recordings from 2-10 HPI were made on PEG-NPs with DS 3.7 and 6.1 (shown in Figures S8-S9). The PEG-NPs DS 3.7 (lamellar ultrastructure) left the bloodstream between 6 to 8 hours post-injection, and the DS 6.1 (hexagonal ultrastructure) was still observed in circulation at 10 hours post-injection, which is in accord with several studies showing that PEGylation increases circulation time (Zalipsky et al., 1994). The faster clearance observed for PEG-NPs of DS 3.7 compared to PEG-NPs of DS 6.1 also correlates with the higher complement activation factor observed for the former. On the other hand, one timelapse was also performed on a batch of non-PEGylated NPs with DS 4.5 (Figure S10). It showed that, in sharp contrast with PEG-NPs, the non-PEGylated NPs left the bloodstream between 2 to 4 hours post-injection, which is consistent with the high-level complement activation observed for non-PEGylated NPs (Figure 6.D).

To summarize, we have observed that PEGylation is crucial to achieve an increased circulation time, with non-PEGylated NPs being cleared from circulation as early as 4 HPI. Furthermore, the spherically shaped DS 3.7 and 14.6 appeared to form aggregates which were not cleared from circulation by the macrophages, but it is unsure whether these aggregates would be able to exit the blood stream or enter cells for drug delivery. PEG-NPs of DS 6.1 demonstrated the longest circulation time in the timelapse experiment, still being present at 10 HPI. No aggregates were observed from the NP after 48 HPI when they appeared to be completely engulfed by macrophages.

4. Conclusion

This study has demonstrated the possibility of synthesizing amphiphilic cyclodextrins in an easy and predictable manner, in contrast to the multi-step processes involving alcohol protection and deprotection that had previously been used. By choosing the right catalyst, it was possible to target a specific DS and thereby produce an amphiphilic derivative that would self-organize into NPs of defined ultrastructure, that could maintain their morphology after PEGylation. No apparent toxicity was observed for these NPs regardless of their size and structure, and those organized as an inverse hexagonal phase showed a longer circulating time. While this study focused on the production and characterization of empty NPs without active substances, it has paved the way for assessing their effectiveness in encapsulating and delivering drugs. The progress made provides a foundation for promising projects in the future.

Acknowledgements

Luc AUGIS acknowledges the French National Research Agency for his doctoral scholarship. The authors would like to thank Fang-Ching CHAO for providing training on complement activation. The authors acknowledge Bastien PROST from IPSIT, SAMM Facility, for his support in LCMS analysis. We acknowledge Karine LEBLANC for the elemental analysis and Cédric PRZYBYLSKI for mass spectrometry. We acknowledge Gillian BARRATT for her careful reading. We acknowledge Cyclolab® for providing few modified cyclodextrins. We also acknowledge the Mass Spectrometry Core Facility of Sorbonne Université (MS3U). This work was partially supported by the "PHC AURORA" program (project number: 47036VD), funded by the French Ministry for Europe and Foreign Affairs, the French Ministry for Higher Education and Research and the Norvegian Council for Research. The zebrafish biodistribution imaging was performed at the Molecular Imaging Center (MIC) Department of Biomedicine, University of Bergen, and zebrafish embryo and E3 medium was acquired at the Zebrafish Facility, Department of Biological Sciences, University of Bergen. Use of the Stanford Synchrotron Radiation Lightsource, SLAC National Accelerator Laboratory, is supported by the U.S. Department of Energy, Office of Science, Office of Basic Energy Sciences under Contract No. DE-AC02-76SF00515. The SSRL Structural Molecular Biology Program is supported by the DOE Office of Biological and Environmental Research, and by the National Institutes of Health, National Institute of General Medical Sciences (P30GM133894). The contents of this publication are solely the responsibility of the authors and do not necessarily represent the official views of NIGMS or NIH. The Pilatus detector at beamline 4-2 at SSRL was funded under National Institutes of Health Grant S10OD021512.

CRediT authorship contribution statement

Luc Augis: Methodology, Formal analysis, Investigation, Writing – Original Draft, Writing - Review & Editing, Visualization; **Ingeborg Nerbø Reiten**: Methodology, Formal analysis, Investigation, Writing - Review & Editing; **Jan-Lukas Førde**: Methodology, Formal analysis, Investigation, Writing - Review & Editing; **Juan M. Casas-Solvas**: Investigation, Resources, Writing - Review & Editing; **Christina Sizun**: Investigation, Writing - Review & Editing; **Thomas Bizien**: Investigation, Writing - Review & Editing; **Ivan Rajkovic**: Investigation, Writing - Review & Editing; **Eric Larquet:** Investigation, Writing - Review & Editing; **Alexandre Michelet:** Investigation, Writing - Review & Editing; **Mayeul Collot**: Resources, Writing - Review & Editing; **Sylviane Lesieur:** Writing - Review & Editing; **Lars Herfindal:** Methodology, Writing - Review & Editing, Supervision; **François-Xavier Legrand:** Conceptualization, Methodology, Formal analysis, Writing - Review & Editing, Supervision, Project administration, Funding acquisition.

Conflicts of Interest

The authors declare that they have no known competing financial interests or personal relationships that could have appeared to influence the work reported in this paper.

References

Addgene URL https://www.addgene.org/58935/ (accessed 4.17.23).

Aytac, Z., Uyar, T., 2016. Antioxidant activity and photostability of α-tocopherol/β-cyclodextrin inclusion complex encapsulated electrospun polycaprolactone nanofibers. Eur. Polym. J. 79, 140–149. https://doi.org/10.1016/j.eurpolymj.2016.04.029

B. Brady, N. Lynam, T. O'Sullivan, C. Ahern, R. Darcy, 2000. 6A-O-p-Toluenesulfonyl-β-cyclodextrin. Org. Synth. 77, 220–221. https://doi.org/10.15227/orgsyn.077.0220

Bandi, S.P., Kumbhar, Y.S., Venuganti, V.V.K., 2020. Effect of particle size and surface charge of nanoparticles in penetration through intestinal mucus barrier. J. Nanoparticle Res. 22, 62. https://doi.org/10.1007/s11051-020-04785-y

Benito, J.M., García Fernández, J.M., 2019. Protecting Groups: Strategies and Applications in Carbohydrate Chemistry, 1st ed. Wiley. https://doi.org/10.1002/9783527697014

Benkovics, G., Malanga, M., Cutrone, G., Béni, S., Vargas-Berenguel, A., Casas-Solvas, J.M., 2021. Facile synthesis of per(6-O-tert-butyldimethylsilyl)-α-, β-, and γ-cyclodextrin as protected intermediates for the functionalization of the secondary face of the macrocycles. Nat. Protoc. 16, 965–987. https://doi.org/10.1038/s41596-020-00443-8

Bertholon, I., Vauthier, C., Labarre, D., 2006. Complement Activation by Core–Shell Poly(isobutylcyanoacrylate)–Polysaccharide Nanoparticles: Influences of Surface Morphology, Length, and Type of Polysaccharide. Pharm. Res. 23, 1313–1323. https://doi.org/10.1007/s11095-006-0069-0

Boackle, R.J., Caughman, G.B., Vesely, J., Medgyesi, G., Fudenberg, H.H., 1983. Potentiation of factor H by heparin: A rate-limiting mechanism for inhibition of the alternative complement pathway. Mol. Immunol. 20, 1157–1164. https://doi.org/10.1016/0161-5890(83)90139-6

Bonnet, V., Duval, R., Tran, V., Rabiller, C., 2003. Mono-N-glycosidation of β-Cyclodextrin− Synthesis of 6-(β-Cyclodextrinylamino)-6-deoxy-D-galactosides and of N-(6-Deoxy-β-cyclodextrinyl)galacto-azepane. Eur. J. Org. Chem. 2003, 4810–4818. https://doi.org/10.1002/ejoc.200300449

Challa, R., Ahuja, A., Ali, J., Khar, R.K., 2005. Cyclodextrins in drug delivery: An updated review. AAPS PharmSciTech 6, E329–E357. https://doi.org/10.1208/pt060243

Chithrani, B.D., Ghazani, A.A., Chan, W.C.W., 2006. Determining the Size and Shape Dependence of Gold Nanoparticle Uptake into Mammalian Cells. Nano Lett. 6, 662–668. https://doi.org/10.1021/nl052396o

Choisnard, L., Gèze, A., Putaux, J.-L., Wong, Y.-S., Wouessidjewe, D., 2006. Nanoparticles of β-Cyclodextrin Esters Obtained by Self-Assembling of Biotransesterified β-Cyclodextrins. Biomacromolecules 7, 515–520. https://doi.org/10.1021/bm0507655

Cold Spring Harb Protoc [WWW Document], 2011. . Cold Spring Harb. Protoc. URL http://cshprotocols.cshlp.org/content/2011/10/pdb.rec66449 (accessed 3.21.23).

Couvreur, P., Vauthier, C., 2006. Nanotechnology: Intelligent Design to Treat Complex Disease. Pharm. Res. 23, 1417–1450. https://doi.org/10.1007/s11095-006-0284-8

David, G., Pérez, J., 2009. Combined sampler robot and high-performance liquid chromatography: a fully automated system for biological small-angle X-ray scattering experiments at the Synchrotron SOLEIL SWING beamline. J. Appl. Crystallogr. 42, 892–900. https://doi.org/10.1107/S0021889809029288

Davis, M.E., Brewster, M.E., 2004. Cyclodextrin-based pharmaceutics: past, present and future. Nat. Rev. Drug Discov. 3, 1023–1035. https://doi.org/10.1038/nrd1576

De Gaetano, F., Scala, A., Celesti, C., Lambertsen Larsen, K., Genovese, F., Bongiorno, C., Leggio, L., Iraci, N., Iraci, N., Mazzaglia, A., Ventura, C.A., 2023. Amphiphilic Cyclodextrin Nanoparticles as Delivery System for Idebenone: A Preformulation Study. Molecules 28, 3023. https://doi.org/10.3390/molecules28073023

Debouzy, J.C., Crouzier, D., Dabouis, V., Gadelle, A., 2008. Caractérisation physicochimique du dérivé amphiphile per(6-déoxy) de la bêta-cyclodextrine (B6) et étude de son activité hémolytique et de son action vis-à-vis des membranes. Ann. Pharm. Fr. 66, 19–27. https://doi.org/10.1016/j.pharma.2007.10.001

Des Prez, R.M., Bryan, C.S., Hawiger, J., Colley, D.G., 1975. Function of the Classical and Alternate Pathways of Human Complement in Serum Treated with Ethylene Glycol Tetraacetic Acid and MgCl2-Ethylene Glycol Tetraacetic Acid. Infect. Immun. 11, 1235–1243. https://doi.org/10.1128/iai.11.6.1235-1243.1975

Dicke, R., 2004. A straight way to regioselectively functionalized polysaccharide esters. Cellulose 11, 255–263. https://doi.org/10.1023/B:CELL.0000025426.82260.71

Duncan, R., Gaspar, R., 2011. Nanomedicine(s) under the Microscope. Mol. Pharm. 8, 2101–2141. https://doi.org/10.1021/mp200394t

Falvey, P., Lim, C.W., Darcy, R., Revermann, T., Karst, U., Giesbers, M., Marcelis, A.T.M., Lazar, A., Coleman, A.W., Reinhoudt, D.N., Ravoo, B.J., 2005. Bilayer Vesicles of Amphiphilic Cyclodextrins: Host Membranes That Recognize Guest Molecules. Chem. – Eur. J. 11, 1171–1180. https://doi.org/10.1002/chem.200400905

Førde, J.-L., Reiten, I.N., Fladmark, K.E., Kittang, A.O., Herfindal, L., 2022. A new software tool for computer assisted *in vivo* high-content analysis of transplanted fluorescent cells in intact zebrafish larvae. Biol. Open 11, bio059530. https://doi.org/10.1242/bio.059530

Fügedi, P., 1989. Synthesis of heptakis(6-O-tert-butyldimethylsilyl)cyclomaltoheptaose and octakis(6-O-tert-butyldimethylsilyl)cyclomaltooctaose. Carbohydr. Res. 192, 366–369. https://doi.org/10.1016/0008-6215(89)85197-3

Gaidamauskas, E., Norkus, E., Butkus, E., Crans, D.C., Grincienė, G., 2009. Deprotonation of β-cyclodextrin in alkaline solutions. Carbohydr. Res. 344, 250–254. https://doi.org/10.1016/j.carres.2008.10.025

Geze, A., Aous, S., Baussanne, I., Putaux, J., Defaye, J., Wouessidjewe, D., 2002. Influence of chemical structure of amphiphilic b-cyclodextrins on their ability to form stable nanoparticles. Int. J. Pharm. 242, 301–305. https://doi.org/10.1016/S0378-5173(02)00192-8

Huang, X., Li, L., Liu, T., Hao, N., Liu, H., Chen, D., Tang, F., 2011. The Shape Effect of Mesoporous Silica Nanoparticles on Biodistribution, Clearance, and Biocompatibility *in Vivo*. ACS Nano 5, 5390–5399. https://doi.org/10.1021/nn200365a

Irie, T., Uekama, K., 1997. Pharmaceutical Applications of Cyclodextrins. III. Toxicological Issues and Safety Evaluation. J. Pharm. Sci. 86, 147–162. https://doi.org/10.1021/js960213f

Jiménez Blanco, J.L., Benito, J.M., Ortiz Mellet, C., García Fernández, J.M., 2017. Molecular nanoparticle-based gene delivery systems. J. Drug Deliv. Sci. Technol. 42, 18–37. https://doi.org/10.1016/j.jddst.2017.03.012

Kauscher, U., Stuart, M.C.A., Drücker, P., Galla, H.-J., Ravoo, B.J., 2013. Incorporation of Amphiphilic Cyclodextrins into Liposomes as Artificial Receptor Units. Langmuir 29, 7377–7383. https://doi.org/10.1021/la3045434

Khalil, R.A., Zarari, A.A., 2014. Theoretical estimation of the critical packing parameter of amphiphilic self-assembled aggregates. Appl. Surf. Sci. 318, 85–89. https://doi.org/10.1016/j.apsusc.2014.01.046

Khan, F., 2022. Nanotechnology in Diagnosis. Int. J. Sci. Res. 8, 2074–2079.

Kher, C., Kumar, S., 2022. The Application of Nanotechnology and Nanomaterials in Cancer Diagnosis and Treatment: A Review. Cureus. https://doi.org/10.7759/cureus.29059

Kimmel, C.B., Ballard, W.W., Kimmel, S.R., Ullmann, B., Schilling, T.F., 1995. Stages of embryonic development of the zebrafish. Dev. Dyn. 203, 253–310. https://doi.org/10.1002/aja.1002030302

Komiyama, M., 2023. Cyclodextrins as eminent constituents in nanoarchitectonics for drug delivery systems. Beilstein J. Nanotechnol. 14, 218–232. https://doi.org/10.3762/bjnano.14.21

Law, H., Benito, J.M., García Fernández, J.M., Jicsinszky, L., Crouzy, S., Defaye, J., 2011. Copper(II)-Complex Directed Regioselective Mono-p-Toluenesulfonylation of Cyclomaltoheptaose at a Primary Hydroxyl Group Position: An NMR and Molecular Dynamics-Aided Design. J. Phys. Chem. B 115, 7524–7532. https://doi.org/10.1021/jp2035345

Lemos-Senna, E., Wouessidjewe, D., Lesieur, S., Puisieux, F., Couarraze, G., Duchĕne, D., 1998. Evaluation of the Hydrophobic Drug Loading Characteristics in Nanoprecipitated Amphiphilic Cyclodextrin Nanospheres. Pharm. Dev. Technol. 3, 85–94. https://doi.org/10.3109/10837459809028482

Lesieur, S., Charon, D., Lesieur, P., Ringard-Lefebvre, C., Muguet, V., Duchêne, D., Wouessidjewe, D., 2000. Phase behavior of fully hydrated DMPC-amphiphilic cyclodextrin systems. Chem. Phys. Lipids 106, 127–144. https://doi.org/10.1016/S0009-3084(00)00149-3

Lin, Y.-S., Haynes, C.L., 2010. Impacts of Mesoporous Silica Nanoparticle Size, Pore Ordering, and Pore Integrity on Hemolytic Activity. J. Am. Chem. Soc. 132, 4834–4842. https://doi.org/10.1021/ja910846q

Loftsson, T., Brewster, M.E., 2012. Cyclodextrins as Functional Excipients: Methods to Enhance Complexation Efficiency. J. Pharm. Sci. 101, 3019–3032. https://doi.org/10.1002/jps.23077

Malvern 2017. URL https://www.malvernpanalytical.com/en/learn/knowledge-center/whitepapers/wp111214dlstermsdefined (accessed 3.15.23).

Martel, A., Liu, P., Weiss, T.M., Niebuhr, M., Tsuruta, H., 2012. An integrated high-throughput data acquisition system for biological solution X-ray scattering studies. J. Synchrotron Radiat. 19, 431–434. https://doi.org/10.1107/S0909049512008072

Maynard, D.K., Vigh, G., 2000. Synthesis and analytical characterization of the sodium salt of heptakis(2-O-methyl-3,6-di-O-sulfo)cyclomaltoheptaose, a chiral resolving agent candidate for capillary electrophoresis. Carbohydr. Res. 328, 277–285. https://doi.org/10.1016/S0008-6215(00)00114-2

McNicholas, S., Rencurosi, A., Lay, L., Mazzaglia, A., Sturiale, L., Perez, M., Darcy, R., 2007. Amphiphilic *N* -Glycosyl-thiocarbamoyl Cyclodextrins: Synthesis, Self-Assembly, and Fluorimetry of Recognition by *Lens culinaris* Lectin. Biomacromolecules 8, 1851–1857. https://doi.org/10.1021/bm070055u

Memişoğlu, E., Bochot, A., Şen, M., Charon, D., Duchêne, D., Hıncal, A.A., 2002. Amphiphilic β-Cyclodextrins Modified on the Primary Face: Synthesis, Characterization, and Evaluation of Their Potential as Novel Excipients in the Preparation of Nanocapsules. J. Pharm. Sci. 91, 1214–1224. https://doi.org/10.1002/jps.10105

Memisoglu-Bilensoy, E., Vural, I., Bochot, A., Renoir, J.M., Duchene, D., Hıncal, A.A., 2005. Tamoxifen citrate loaded amphiphilic β-cyclodextrin nanoparticles: In vitro characterization and cytotoxicity. J. Controlled Release 104, 489–496. https://doi.org/10.1016/j.jconrel.2005.03.006

Mendez-Ardoy, A., Gomez-Garcia, M., Geze, A., Putaux, J.-L., Wouessidjewe, D., Ortiz Mellet, C., Defaye, J., M. Garcia Fernandez, J., M. Benito, J., 2012. Monodisperse Nanoparticles from Self-Assembling Amphiphilic Cyclodextrins: Modulable Tools for the Encapsulation and Controlled Release of Pharmaceuticals. Med. Chem. 8, 524–532. https://doi.org/10.2174/157340612801216265

Mohan Nalluri, S.K., Bultema, J.B., Boekema, E.J., Ravoo, B.J., 2011. Metal ion responsive adhesion of vesicles by conformational switching of a non-covalent linker. Chem. Sci. 2, 2383. https://doi.org/10.1039/c1sc00422k

Morille, M., Montier, T., Legras, P., Carmoy, N., Brodin, P., Pitard, B., Benoît, J.-P., Passirani, C., 2010. Long-circulating DNA lipid nanocapsules as new vector for passive tumor targeting. Biomaterials 31, 321–329. https://doi.org/10.1016/j.biomaterials.2009.09.044

Olmstead, W.N., Margolin, Z., Bordwell, F.G., 1980. Acidities of water and simple alcohols in dimethyl sulfoxide solution. J. Org. Chem. 45, 3295–3299. https://doi.org/10.1021/jo01304a032

Parsons, R., 1967. Atlas of electrochemical equilibria in aqueous solutions. J. Electroanal. Chem. Interfacial Electrochem. 13, 471. https://doi.org/10.1016/0022-0728(67)80059-7

Perret, P., Bacot, S., Gèze, A., Gentil Dit Maurin, A., Debiossat, M., Soubies, A., Blanc-Marquis, V., Choisnard, L., Boutonnat, J., Ghezzi, C., Putaux, J.L., Lancelon-Pin, C.,

Riou, L.M., Wouessidjewe, D., 2018. Biodistribution and preliminary toxicity studies of nanoparticles made of Biotransesterified β–cyclodextrins and PEGylated phospholipids. Mater. Sci. Eng. C 85, 7–17. https://doi.org/10.1016/j.msec.2017.12.017

Putaux, J.-L., Lancelon-Pin, C., Legrand, F.-X., Pastrello, M., Choisnard, L., Gèze, A., Rochas, C., Wouessidjewe, D., 2017. Self-Assembly of Amphiphilic Biotransesterified β-Cyclodextrins: Supramolecular Structure of Nanoparticles and Surface Properties. Langmuir 33, 7917–7928. https://doi.org/10.1021/acs.langmuir.7b01136

Quaglia, F., Ostacolo, L., Mazzaglia, A., Villari, V., Zaccaria, D., Sciortino, M.T., 2009. The intracellular effects of non-ionic amphiphilic cyclodextrin nanoparticles in the delivery of anticancer drugs. Biomaterials 30, 374–382. https://doi.org/10.1016/j.biomaterials.2008.09.035

Raffaini, G., Ganazzoli, F., 2007. Hydration and flexibility of α-, β-, γ- and δ-cyclodextrin: A molecular dynamics study. Chem. Phys. 333, 128–134. https://doi.org/10.1016/j.chemphys.2007.01.015

Rong, D., D'Souza, V.T., 1990. A convenient method for functionalization of the 2-position of cyclodextrins. Tetrahedron Lett 31, 4275–4278. https://doi.org/10.1016/S0040-4039(00)97599-3

Rossini, E., Bochevarov, A.D., Knapp, E.W., 2018. Empirical Conversion of p pKa Values between Different Solvents and Interpretation of the Parameters: Application to Water, Acetonitrile, Dimethyl Sulfoxide, and Methanol. ACS Omega 3, 1653–1662. https://doi.org/10.1021/acsomega.7b01895

Samanta, A., Stuart, M.C.A., Ravoo, B.J., 2012. Photoresponsive Capture and Release of Lectins in Multilamellar Complexes. J. Am. Chem. Soc. 134, 19909–19914. https://doi.org/10.1021/ja3101837

Schindelin, J., Arganda-Carreras, I., Frise, E., Kaynig, V., Longair, M., Pietzsch, T., Preibisch, S., Rueden, C., Saalfeld, S., Schmid, B., Tinevez, J.-Y., White, D.J., Hartenstein, V., Eliceiri, K., Tomancak, P., Cardona, A., 2012. Fiji: an open-source platform for biological-image analysis. Nat. Methods 9, 676–682. https://doi.org/10.1038/nmeth.2019

Skiba, M., Duchêne, D., Puisieux, F., Wouessidjewe, D., 1996. Development of a new colloidal drug carrier from chemically-modified cyclodextrins: Nanospheres and influence of physicochemical and technological factors on particle size. Int. J. Pharm. 129, 113–121. https://doi.org/10.1016/0378-5173(95)04272-5

Skiba, M., Morvan, C., Duchene, D., Bordwell, F., Wouessidjewe, D., 1995. Evaluation of gastrointestinal behaviour in the rat of amphiphilic fl-cyclodextrin nanocapsules, loaded with indomethacin. Int. J. Pharm. 126, 275–279. https://doi.org/10.1016/0378-5173(95)04121-4

Slater, J.C., 1964. Atomic Radii in Crystals. J. Chem. Phys. 41, 3199–3204. https://doi.org/10.1063/1.1725697

Srinivasachari, S., Fichter, K.M., Reineke, T.M., 2008. Polycationic β-Cyclodextrin "Click Clusters": Monodisperse and Versatile Scaffolds for Nucleic Acid Delivery. J. Am. Chem. Soc. 130, 4618–4627. https://doi.org/10.1021/ja074597v

Sriram, M.I., Kalishwaralal, K., Barathmanikanth, S., Gurunathani, S., 2012. Size-based cytotoxicity of silver nanoparticles in bovine retinal endothelial cells. Nanosci. Methods 1, 56–77. https://doi.org/10.1080/17458080.2010.547878

Stella, V.J., He, Q., 2008. Cyclodextrins. Toxicol. Pathol. 36, 30–42. https://doi.org/10.1177/0192623307310945

Stoehr, L.C., Gonzalez, E., Stampfl, A., Casals, E., Duschl, A., Puntes, V., Oostingh, G.J., 2011. Shape matters: effects of silver nanospheres and wires on human alveolar epithelial cells. Part. Fibre Toxicol. 8, 36. https://doi.org/10.1186/1743-8977-8-36

Treccani, S., Alongi, J., Manfredi, A., Ferruti, P., Cavalli, R., Raffaini, G., Ranucci, E., 2022. L-Arginine-Derived Polyamidoamine Oligomers Bearing at Both Ends β-Cyclodextrin Units as pH-Sensitive Curcumin Carriers. Polymers 14, 3193. https://doi.org/10.3390/polym14153193

Uekama, K., Hirayama, F., Irie, T., 1998. Cyclodextrin Drug Carrier Systems. Chem. Rev. 98, 2045–2076. https://doi.org/10.1021/cr970025p

Villari, V., Mazzaglia, A., Darcy, R., O'Driscoll, C.M., Micali, N., 2013. Nanostructures of Cationic Amphiphilic Cyclodextrin Complexes with DNA. Biomacromolecules 14, 811–817. https://doi.org/10.1021/bm3018609

Voskuhl, J., Stuart, M.C.A., Ravoo, B.J., 2010. Sugar-Decorated Sugar Vesicles: Lectin–Carbohydrate Recognition at the Surface of Cyclodextrin Vesicles. Chem. – Eur. J. 16, 2790–2796. https://doi.org/10.1002/chem.200902423

Wang, S., Guo, H., Li, Y., Li, X., 2019. Penetration of nanoparticles across a lipid bilayer: effects of particle stiffness and surface hydrophobicity. Nanoscale 11, 4025–4034. https://doi.org/10.1039/C8NR09381D

Wang, X., Bou, S., Klymchenko, A.S., Anton, N., Collot, M., 2021. Ultrabright Green-Emitting Nanoemulsions Based on Natural Lipids-BODIPY Conjugates. Nanomaterials 11, 826. https://doi.org/10.3390/nano11030826

Ward, S., Ling, C.-C., 2011. Efficient and Versatile Modification of the Secondary Face of Cyclodextrins through Copper-Catalyzed Huisgen 1,3-Dipolar Cycloaddition. Eur. J. Org. Chem. 4853–4861. https://doi.org/10.1002/ejoc.201100445

Yaméogo, J.B.G., Gèze, A., Choisnard, L., Putaux, J.-L., Mazet, R., Passirani, C., Keramidas, M., Coll, J.-L., Lautram, N., Bejaud, J., Semdé, R., Wouessidjewe, D., 2014. Self-assembled biotransesterified cyclodextrins as potential Artemisinin nanocarriers. II: In vitro behavior toward the immune system and in vivo biodistribution assessment of unloaded nanoparticles. Eur. J. Pharm. Biopharm. 88, 683–694. https://doi.org/10.1016/j.ejpb.2014.08.012

Zagami, R., Barattucci, A., Monsù Scolaro, L., Viale, M., Raffaini, G., Maria Bonaccorsi, P., Mazzaglia, A., 2023. Curcumin/amphiphilic cyclodextrin nanoassemblies: Theoretical and spectroscopic studies to address their debut in anticancer therapy. J. Mol. Liq. 389, 122841. https://doi.org/10.1016/j.molliq.2023.122841

Zalipsky, S., Brandeis, E., Newman, M.S., Woodle, M.C., 1994. Long circulating, cationic liposomes containing amino-PEG-phosphatidylethanolamine. FEBS Lett. 353, 71–74. https://doi.org/10.1016/0014-5793(94)01013-7

Zhang, J., Ma, P.X., 2013. Cyclodextrin-based supramolecular systems for drug delivery: Recent progress and future perspective. Adv. Drug Deliv. Rev. 65, 1215–1233. https://doi.org/10.1016/j.addr.2013.05.001

Figures

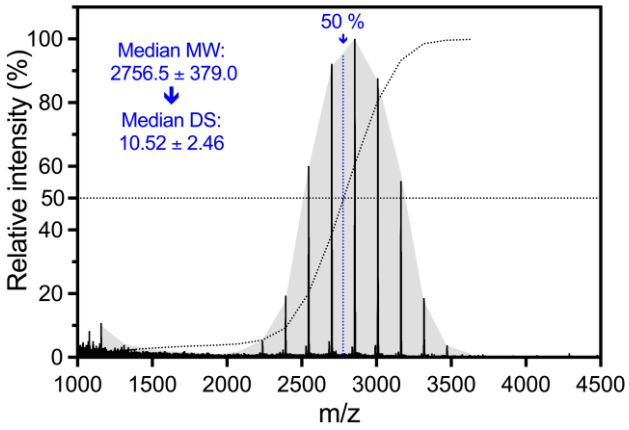

Figure 1. MALDI-MS Spectrum of β-CD-C_{10}-$DS_{10.5}$ derivative. The gray area represents the distribution of the derivative-related peaks. An increasing cumulative frequency curve was established from the intensity of each peak, represented by the dotted curve. A median molecular weight of 2756.5 g.mol^{-1} was measured, with a standard deviation of 379.0 g.mol^{-1}, corresponding to the width at half height calculated by the m/z difference between 75% and 25% frequencies. This leads to a median degree of substitution (DS) of 10.52, with a standard deviation of 2.46.

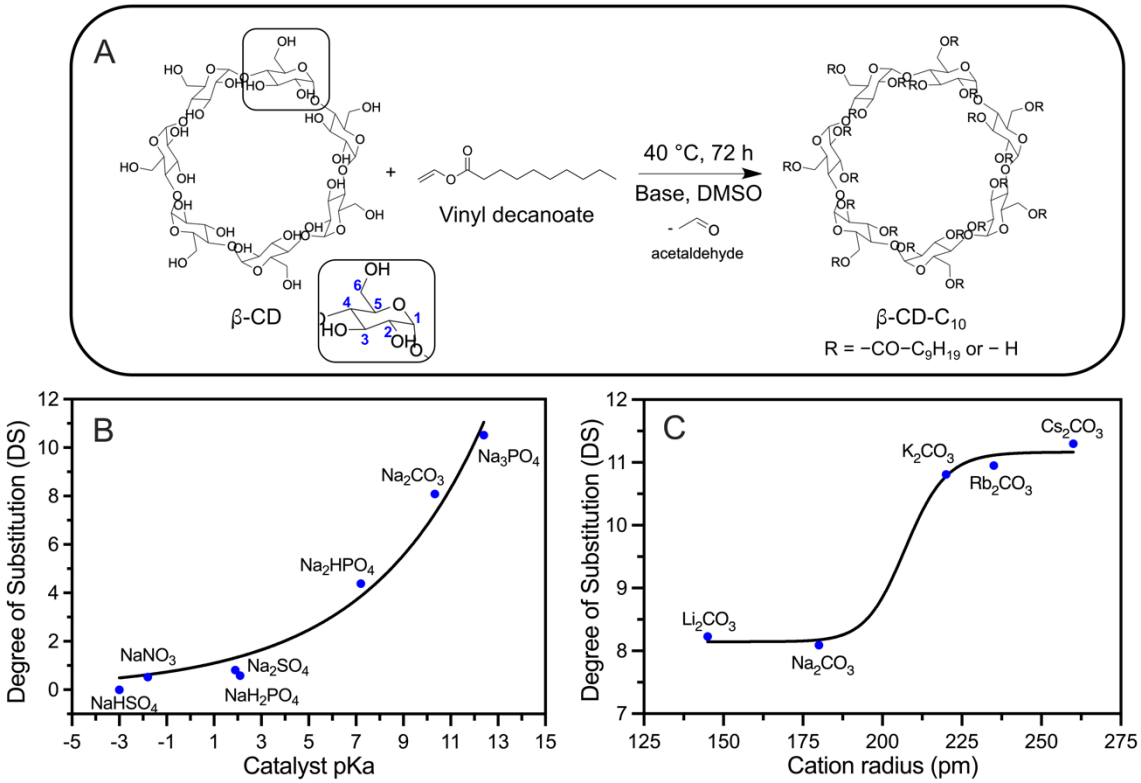

Figure 2. Transesterification reaction of β-CD using vinyl decanoate reagent (A). DS dependence of β-CD-C_{10} derivatives on sodium-based catalyst pKa (B) and on the cationic counter ion radius of carbonate-based catalyst (C). The pKa values were determined based on the relative acid forms (Parsons, 1967) and the atomic radii values were sourced from (Slater, 1964). Exponential (B) and sigmoid (C) fits were applied.

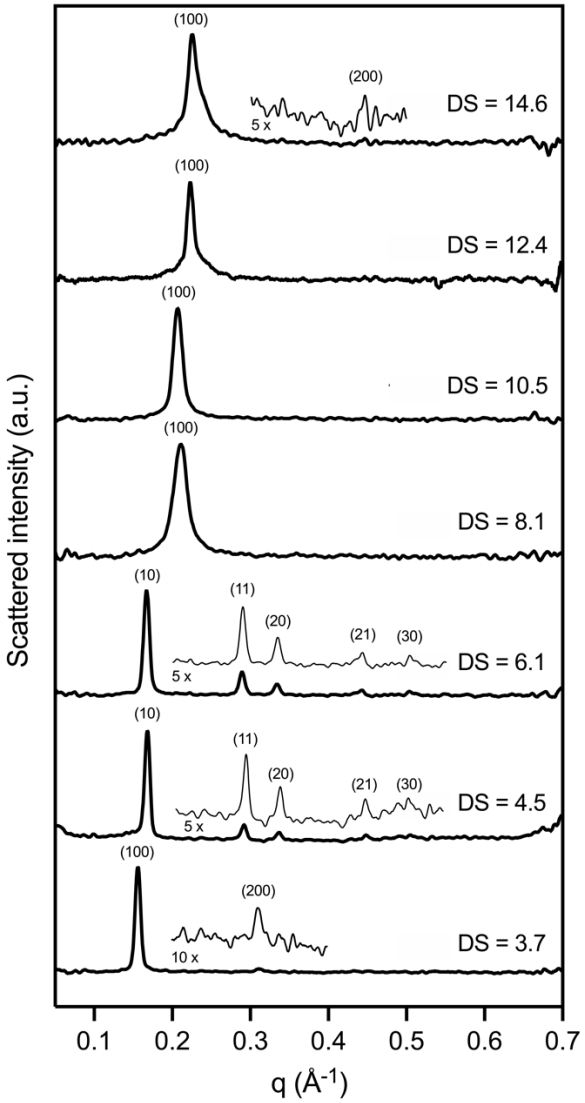

Figure 3. SAXS profiles of β-CD-C_{10} derivatives NPs in aqueous medium from DS 3.7 to 14.6.

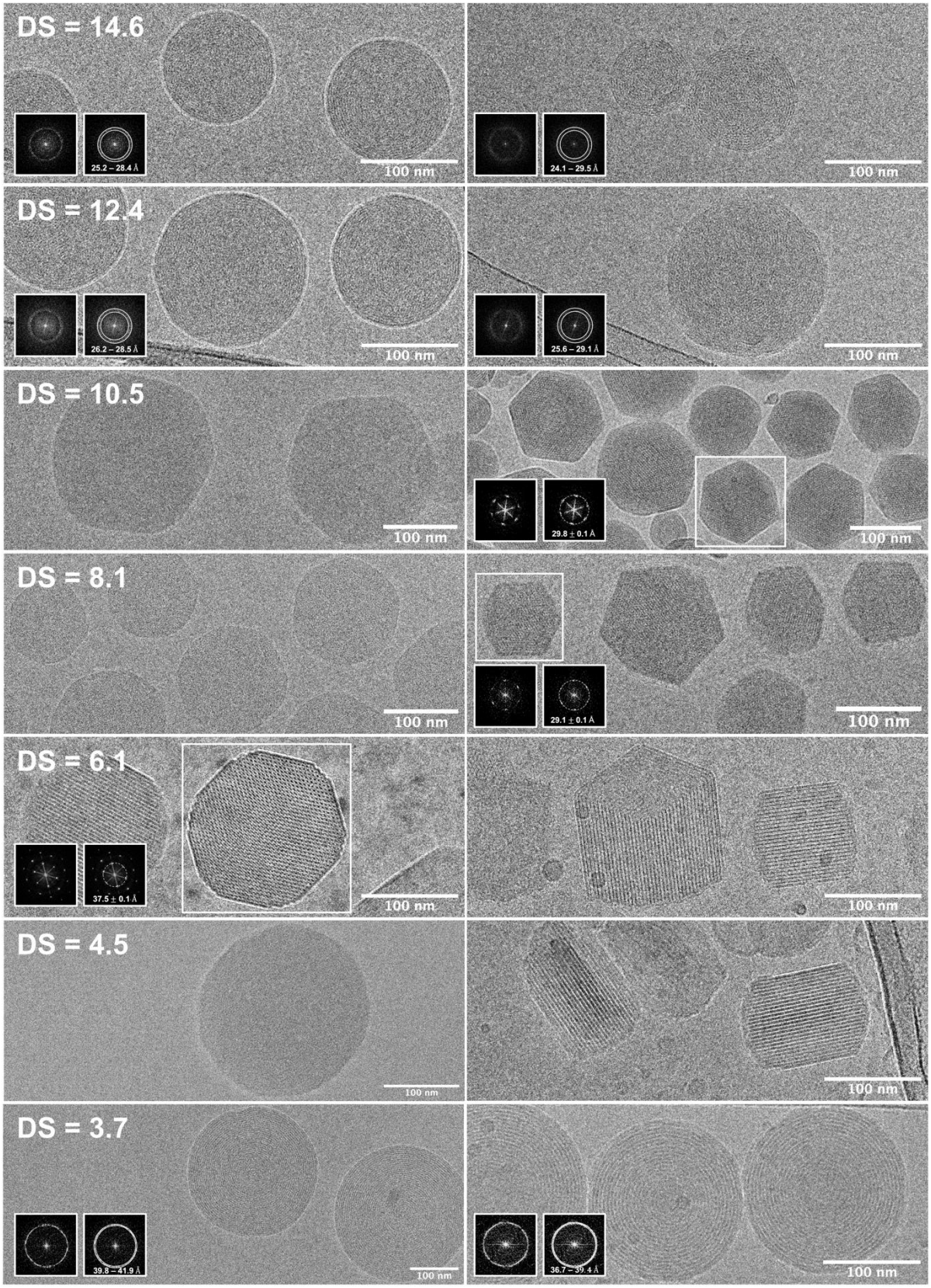

Figure 4. Cryo-EM images of non-PEGylated (left column) and PEGylated (right column) β-CD-C_{10}-NPs in aqueous medium with DS ranging from 3.7 to 14.6 (bottom to top). The inserts display Fourier Transform patterns and provide the corresponding range distance related to the first order.

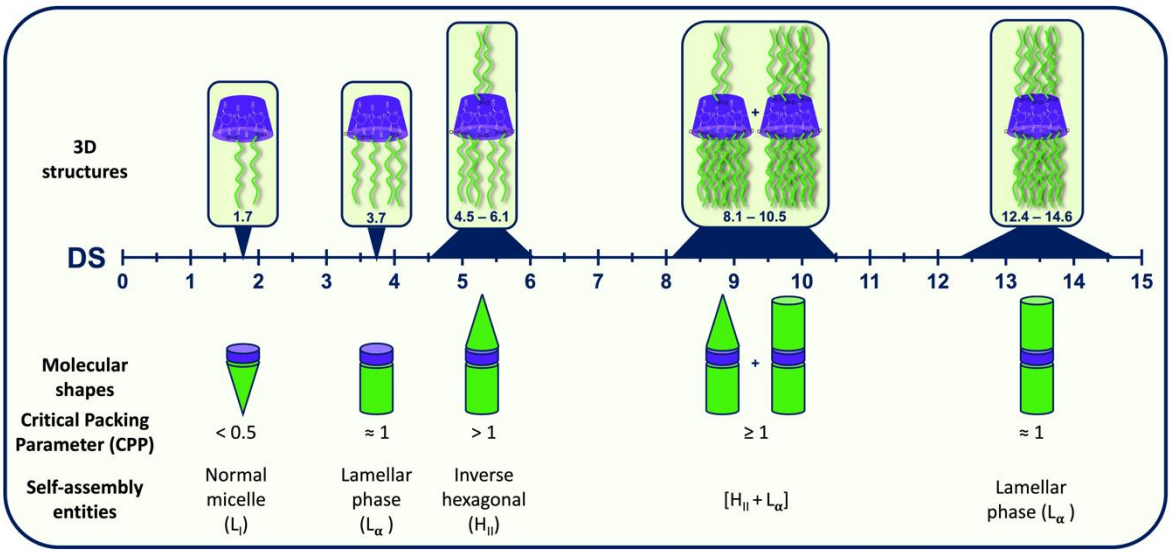

Figure 5. Estimated molecular shapes and critical packing parameter (CPP) values for each derivative according to their degree of substitution. CPP values are assumptions and were not quantified.

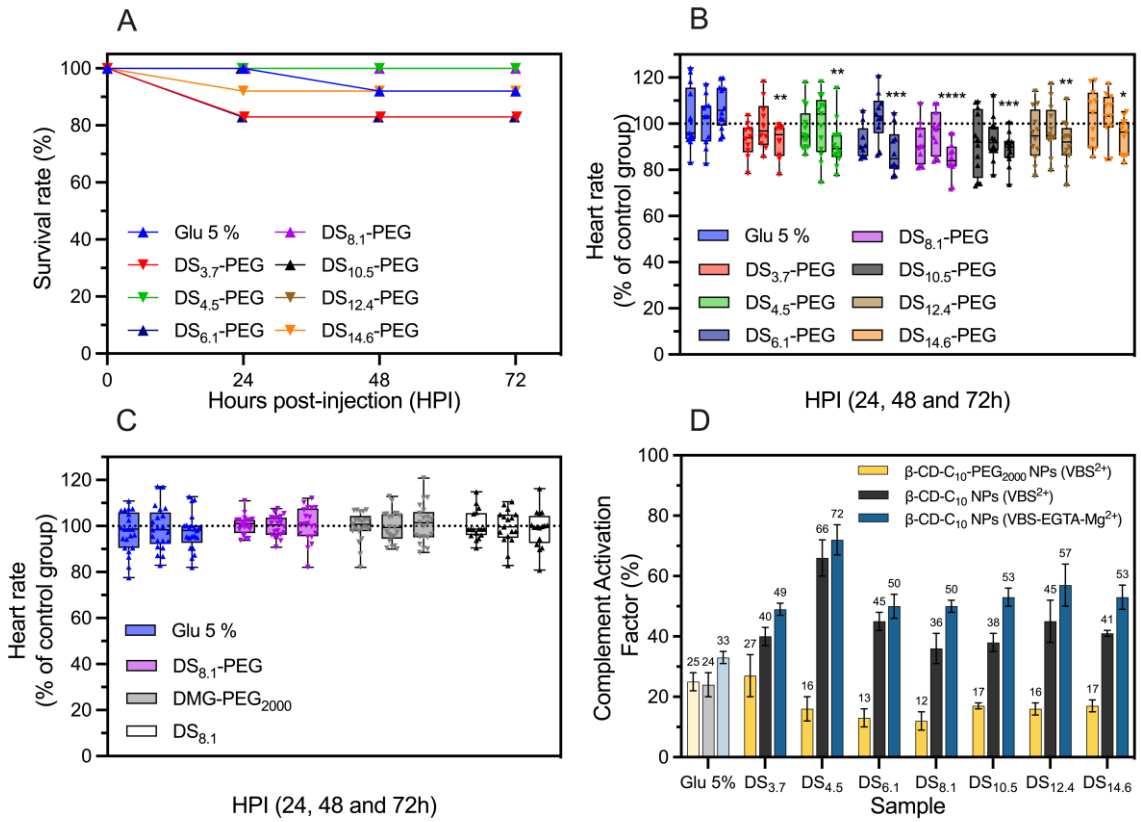

Figure 6. Survival rate (A) and heart rate percentage of control group (B, C) over 3 days post injections of PEGylated β-CD-C_{10} NPs (N = 12/13 for B and N = 22 for C). The first, second and third bars for each group correspond to 24, 48 and 72 HPI. Values from each day are compared with each other. MEA values are shown between Glu 5 % and all the ACD-NPs (*p*-values keys: * = 0.01 ≤ *p* < 0.05, ** = 0.001 ≤ *p* < 0.01, *** = 0.0001 ≤ *p* < 0.001, and **** = *p* < 0.0001). Complement activation (D) of β-CD-C_{10} NPs non-PEGylated (in grey) and PEGylated (in yellow), both using VBS^{2+} as buffer. VBS-EGTA-Mg^{2+} buffer was also used on non-PEGylated NPs (in blue). Displayed values are averages of triplicates.

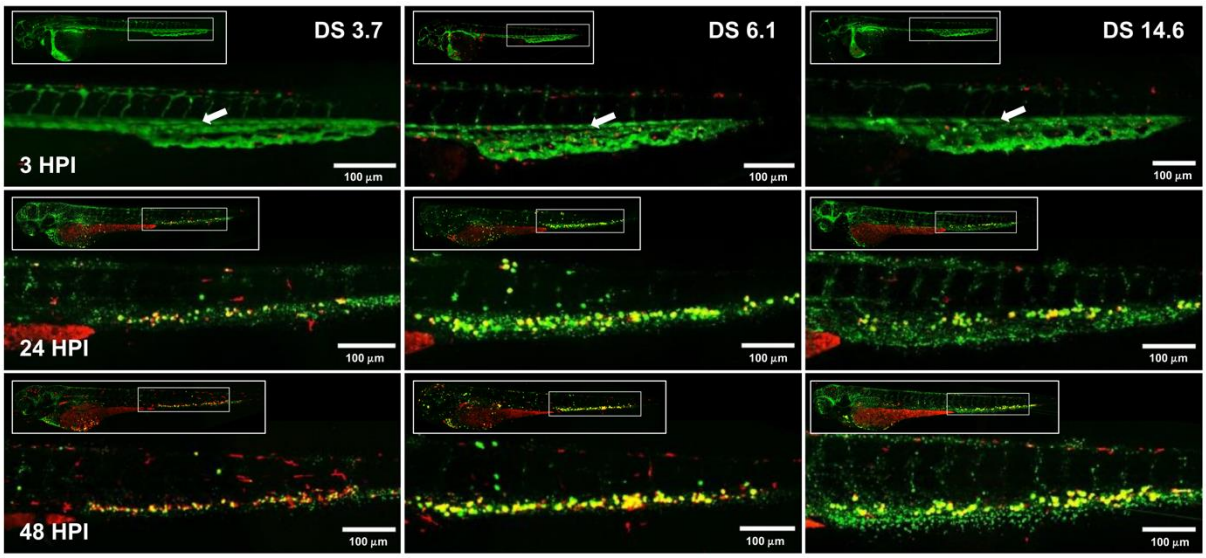

Figure 7. Confocal images focused on the tail portion of mpeg1:mCherry embryos with red fluorescent macrophages injected with PEGylated NPs (green fluorescence). Columns represent DS 3.7, 6.1 and 14.6 NPs, while rows represent the post-injection time, ranging from 3 to 48 hours.

Tables

Table 1. Hydrodynamic diameters and ultrastructure characteristics of seven β-CD-C_{10} NPs prepared in purified water, except for Zeta potential where they were dispersed in glucose 5 %. DLS and Zeta potential values are mean ± S.D. of 3 independent dilutions measured for at least 10 times each. Ultrastructure characteristics were deduced from SAXS patterns and the long-range intermolecular distance calculated from the first-order Bragg reflection.

DS	Nanoparticle hydrodynamic diameter ± S.D. [nm]	PdI	Ultrastructure	Recorded number of Bragg reflections [a]	d_{100} ± S.D. [b] [Å]	a_{hex} ± S.D. [Å]	Zeta potential [mV] [d]
3.7	277 ± 2	0.076	Lamellar	2	39.5 ± 0.6		– 22.8 ± 1.4
4.5	217 ± 1	0.116	Hexagonal	5	37.0 ± 0.2	42.8 ± 0.2	– 11.7 ± 1.5
6.1	158 ± 1	0.037	Hexagonal	5	37.2 ± 0.1	43.1 ± 0.2	– 16.7 ± 1.7
8.1	188 ± 3	0.075	n.d.	1	29.4		– 10.2 ± 0.4
10.5	169 ± 2	0.086	n.d.	1	30.1		– 9.1 ± 1.0
12.4	170 ± 4	0.066	Lamellar [c]	1	28.0		– 28.1 ± 1.3
14.6	172 ± 1	0.096	Lamellar	2	28.0 ± 0.2		– 21.4 ± 0.8

[a] number of diffraction peaks on SAXS patterns
[b] long-range relating to the first order position
[c] ultrastructure was identified by cryo-EM images
[d] prepared in glucose 5 %
n.d.: not determined

Table 2. Hydrodynamic diameters and ultrastructure characteristics of seven PEGylated β-CD-C_{10} NPs prepared in purified water, except for Zeta potential where they were dispersed in glucose 5 %. DLS and Zeta potential values are mean ± S.D. of 3 independent dilutions measured for at least 10 times each. Ultrastructure characteristics were deduced from SAXS patterns and the long-range intermolecular distance calculated from the first-order Bragg reflection.

DS	Nanoparticle hydrodynamic diameter ± S.D. [nm]	PdI	Ultrastructure	Recorded number of Bragg reflections [a]	d_{100} ± S.D. [b] [Å]	a_{hex} ± S.D. [Å]	Zeta potential [mV] [d]
3.7	159 ± 1	0.062	Lamellar	2	39.2 ± 0.5		– 7.2 ± 1.0
4.5	156 ± 3	0.107	Hexagonal	5	39.5 ± 0.1	45.6 ± 0.1	– 5.7 ± 0.6
6.1	158 ± 2	0.083	Hexagonal	6	39.9 ± 0.2	46.0 ± 0.3	– 5.3 ± 0.3
8.1	161 ± 2	0.108	Hexagonal [c]	1	32.4		– 5.0 ± 0.8
10.5	161 ± 0	0.082	Hexagonal	3	32.6 ± 0.3	37.6 ± 0.3	– 8.6 ± 0.9
12.4	162 ± 2	0.117	Lamellar [c]	1	30.1		– 10.3 ± 0.4
14.6	160 ± 1	0.113	Lamellar [c]	1	29.1		– 11.0 ± 0.4

[a] number of diffraction peaks on SAXS patterns
[b] long-range relating to the first order position
[c] ultrastructure was identified by cryo-EM images
[d] prepared in glucose 5 %